COLLIDER PHYSICS

Dorothee Schaile
Ludwig-Maximilians-Universität München, Germany

Abstract

The lecture gives a guided tour through a selection of recent experimental results at our present high energy colliders: Tevatron, SLC, LEP and HERA. The topics covered include electroweak precision tests at the Z^0 resonance, the study of W production, the determination of the strong coupling constant and the observation of the top quark. The variety of these measurements represents a stringent consistency test of our present understanding of the theoretical foundations of particle physics. Their combination imposes important constraints on the parameter space of the Standard Model and possible extensions.

1. Introduction

1.1 Outline of lectures

Colliders are powerful tools in experimental particle physics covering a rich spectrum of outstanding questions. This lecture will focus on a selection of recent results in collider physics which probe the building principle of the the Standard Model: local gauge invariance. After a short overview on colliders, this introductory section provides a summary of the observable consequences of the gauge character of the Standard Model.

In Section 2. we discuss properties and couplings of the Z^0 boson. The e^+e^--collider LEP has just completed the data taking phase at the Z-pole. The LEP statistics provides important measurements of the Z^0 boson properties and the coupling of the Z^0 to fermion pairs. These results are complemented by the e^+e^--collider SLC, which has achieved a significant electron beam polarization.

Until recently the investigation of W boson properties and the self-coupling of electroweak gauge bosons which are discussed in Section 3. have been the exclusive domain of $p\overline{p}$ colliders. LEP has just started data taking in a new exciting energy domain which also allows precise tests of the Standard Model with W boson pairs.

An important aspect in testing the Standard Model which is discussed in Section 4. is the determination of the strong coupling constant, α_s, and its energy dependence. At momentum transfers where strong interactions can be described perturbatively, QCD

should become completely predictive with one single measurement of α_s. Colliders offer a wealth of complementary experimental methods at different energy scales.

Section 5. is devoted to the discovery of the top quark and a precise measurement of its mass at the $p\overline{p}$-collider Tevatron. It will be shown in Section 6. that this success is a very important ingredient when we want to derive conclusions from the combination of all our experimental information concerning the Standard Model. The only parameter that enters our calculations and is not predicted by the Standard Model, nor accessible to a direct measurement yet, is the mass of the Higgs boson. The effect of its mass on measurable quantities is extremely tiny. The proof of its existence, however, is the key to our understanding, why the Standard Model works so well, and will be a milestone of future collider physics.

1.2 Collider and fixed target experiments

In order to understand the break-through of colliders in particle physics I would like to discuss two basic aspects of accelerator design: energy and luminosity.

The kinematics of the collision of two particles can be conveniently expressed by their four-vectors $p_1 = (E_1,\ \vec{p_1})$ and $p_2 = (E_2,\ \vec{p_2})$, where E, m and $\vec{p}$ denote energy, mass and momentum of particle one and two, respectively. For the centre-of-mass-energy, E_{cm}, we get:

$$\begin{aligned} E_{cm} &= :\sqrt{s} && (1)\\ &= \left[(p_1+p_2)^2\right]^{\frac{1}{2}} && (2)\\ &= \left[m_1^2+m_2^2+2(E_1E_2-\vec{p_1}\vec{p_2}\right]^{\frac{1}{2}} && (3) \end{aligned}$$

At colliders the masses of the particles can be neglected, i.e. $m_1,\ m_2 << E_1,\ E_2$:

$$E_{cm} \approx \sqrt{4E_1E_2} \tag{4}$$

Furthermore if both particle beams have the same energy, i.e. $E_1 = E_2 = E_{beam}$:

$$E_{cm} = 2E_{beam}. \tag{5}$$

In fixed target experiments, we have for the target particle $E_2 = m_2$, and using again for the projectile $m_1 << E_1 = E_{beam}$, we get:

$$E_{cm} \approx 2\sqrt{m_2E_{beam}} \tag{6}$$

In conclusion colliders make efficient use of the highest energy that can be achieved, whereas in fixed target mode the effort invested in increasing the beam energy only pays off proportional to $\sqrt{E_{beam}}$ for the centre-of-mass-energy which is available for particle excitation and creation.

Another important parameter for the planning of an accelerator experiment is the luminosity $\mathcal{L}$. It is related to the event rate $n^{\cdot}$ for a process with cross-section σ by the relation:

$$n^{\cdot} = \mathcal{L}\sigma \tag{7}$$

For a collider the luminosity can be expressed in terms of the number of particle bunches n_B, the revolution frequency of one particle bunch f, the number of particles per bunch in each beam N_1 and N_2 and the area of the collision point, A, as:

$$\mathcal{L} = \frac{f n_B N_1 N_2}{A} \tag{8}$$

For fixed target operation the luminosity can be expressed as:

$$\mathcal{L} = \Phi \rho, \tag{9}$$

where Φ stands for the number of particles per second of the incoming beam and ρ for the target area density. In fixed target operation it is easy to obtain high luminosities ($>10^{37}$ $s^{-1}cm^{-2}$) as Avogadro's number enters the target density. The luminosity record for existing high energy colliders belongs to LEP with $\mathcal{L} \approx 2 \cdot 10^{31} s^{-1}cm^{-2}$; luminosities in the range 10^{33} or 10^{34} $s^{-1}cm^{-2}$ are the challenge of future machines. In conclusion, if luminosity rather than energy is the important parameter for your research project, you should plan a fixed target experiment.

1.3 Our Colliders at the energy frontier

1.3.1 LEP

The LEP e^+e^- storage ring started operation in 1989 with four general purpose collider detectors: ALEPH [1], DELPHI [2], L3 [3] and OPAL [4]. In a first phase, LEP 1, the centre-of-mass energy, was kept in an interval of ± 3 GeV around the mass of the Z^0, m_Z, allowing the experiments to collect $\approx 2 \cdot 10^7$ Z^0 decays. In a second phase, LEP 2, which started in summer 1996, E_{cm} was raised above the W pair production threshold by the installation of superconducting RF cavities. A first successful run at intermediate energies of $130 - 140$ GeV in November 1995 allowed each of the experiments to collect ≈ 5 pb^{-1}. In June 1996 E_{cm} was increased to 161 GeV. The approved research program of CERN foresees a step-wise increase of E_{cm} to 192 GeV in 1998.

LEP will be our last high energy e^+e^- storage ring. The reason is due to synchrotron radiation which increases with the fourth power of the beam energy but only inversely proportional to the effective bending radius of the ring. At LEP for $\sqrt{s} = m_Z$ the energy radiated by a single electron each turn amounts to 125 MeV [5].

1.3.2 SLC

The next generation e^+e^- collider will be a linear collider. SLC can be viewed as a first e^+e^- linear collider prototype. Electrons and positrons are accelerated simultaneously in an extension of the previously existing SLAC linear collider and then transferred into two separate arcs which guide them to the head-on collision point in the final focus. The interactions are recorded by a single experiment, initially by the MARK II detector [6] and then by the SLD detector [7].

Also SLC started operation in 1989 at $E_{cm} = m_Z$, but its operation is very complementary to LEP 1: They have low statistics, $\approx 140 \cdot 10^3$ Z^0 decays up to now, but a striking success with the electron beam polarization which has reached a record value of 80%.

1.3.3 TEVATRON

The $p\overline{p}$ collider Tevatron started operation in 1987 and takes data at E_{cm} = 1.8 TeV, now at a peak luminosity of $\approx 10^{31}$ cm^{-2}s^{-1}. Data taking has paused in February 1996 when the machine had delivered an integrated luminosity of ≈ 150 pb^{-1}. At present a major machine upgrade is performed which will allow the two experiments, CDF [8] and DØ [9], to restart operation at a substantially increased luminosity in 1999.

The Tevatron will definitively not be the last high energy hadron storage ring. In 2005 LHC is expected to take up operation in the LEP tunnel with 7 TeV protons colliding on 7 TeV protons.

1.3.4 HERA

HERA at DESY, our first and unique ep collider, started operation in 1990. Electrons or positrons at a beam energy of 30 GeV are brought into collision with protons at an energy of 820 GeV. The maximum centre-of-mass energy which can be achieved in collisions of $e^{\pm}$ with one of the constituents of the protons amounts to $E_{cm} = 314$ GeV. The $e^{\pm}$ ring and the proton ring are located in a common tunnel with a circumference of 6.3 km. There are two large general purpose collider experiments, H1 [10] and ZEUS [11], and two specialized experiments: the HERMES experiment is recording collisions of the polarized $e^{\pm}$ beam on a polarized gas-jet target and the planned HERA-B experiment will investigate the collisions of the proton beam halo on a wire target with the aim to detect CP violation in the b quark sector.

1.4 The Standard Model and the role of colliders

The present Standard Model of particle physics is a theory based on the principle of local gauge invariance. The underlying experimental consequences are:

- The existence of the gauge bosons: γ, W^+, W^-, Z^0 and 8 gluons. The heavy intermediate vector bosons have been discovered in 1982 at the CERN $Sp\overline{p}S$ [12] and striking evidence for the existence of gluons was provided in 1979 by the observation of 3-jet events at PETRA [13].
- The existence of an elementary scalar particle, the Higgs boson. The Standard Model predicts the existence but not the mass of this particle. At LEP 1 this particle could be systematically excluded in the mass range 0-66 GeV. An upper experimental bound on its mass of a few hundred GeV can be obtained from the combination of electroweak precision tests with the direct determination of the top quark mass (c.f. Section 6.). LEP 2 extends the discovery limit for the Standard Model Higgs boson to masses up to 95 GeV and has a promising potential for finding one of the two light Higgs bosons predicted by the minimal supersymmetric extension of the Standard Model. The detailed understanding of the Higgs mechanism constitutes a major motivation of future accelerators.
- The theory allows to calculate predictions to all orders of perturbation theory with only a finite number of parameters. As there are only few parameters in the Standard Model which matter at high energies we obtain powerful tests of the theory by probing the relation of observables. Colliders make an important contribution in the following areas:
  - The verification of the predicted multiplet structure of particles
  - The study of the properties of gauge bosons

- The determination of strong and electroweak couplings of gauge bosons to fermions
- The determination of gauge boson self couplings

A very important feature of gauge theories is that higher order corrections to observables can be calculated. Today, this may appear as something self-understood to students in high energy physics. We should keep in mind, however, that the Fermi theory of weak interactions was used as a successful description of experimental data for several decades though it had not this property. Measuring the size of higher order radiative corrections is an important goal of precision tests at LEP and SLC. A milestone whether the theory can be confirmed at quantum level is the comparison of the value of m_{t} derived from precision tests (c.f. discussion on radiative corrections in section 2.1.3) and its direct determination at the Tevatron and future colliders.

Last but not least, colliders play a fundamental role in direct searches for particles which are not predicted by the multiplet structure of the Standard Model. For reasons of time, and as these particles exist only in theory yet, I will not cover these searches in my lectures.

2. Z^0 properties and couplings

2.1 Scan of the Z^0 resonance curve at LEP

Important parameters of the Z^0, especially its mass, m_{Z}, and its total decay width, Γ_{Z}, are obtained from a scan of the Z^0 resonance curve. The results are based on the measurement of the energy dependence of total and differential cross sections as function of centre-of-mass energy for the processes $\mathrm{e}^+\mathrm{e}^- \to$ hadrons and $\mathrm{e}^+\mathrm{e}^- \to \ell^+\ell^-$.

2.1.1 Total cross sections

Total cross sections are determined from experiments via the relation:

$$\sigma(E_{cm}) = \frac{N_{sel} - N_{bg}}{\epsilon \int \mathcal{L} dt} \,,$$

where N_{sel} and N_{bg} refer to the number of events passing the selection cuts and the number of background events in the selected sample. $\int \mathcal{L} dt$ denotes the integrated luminosity and the correction factor ϵ accounts for the trigger efficiency, the geometrical acceptance and the efficiency of the selection cuts.

The design of the LEP detectors allows a trigger on hadrons and leptons with high redundancy, accepting 100% of the events, with an uncertainty of less than 0.1%, within the solid angle considered in the analysis.

The selection of hadrons and lepton pairs at LEP is conceptually easy, as they can be discriminated by a few simple cuts like cluster or track multiplicities, deposited energy and energy balance, against backgrounds which are of $\mathcal{O}(0.1\%)$ for hadrons and $\mathrm{e}^+\mathrm{e}^-$ pairs, of $\mathcal{O}(1\%)$ for $\mu^+\mu^-$ and$\tau^+\tau^-$ pairs. The challenge of the analysis is motivated by the aim to match the systematic error of the efficiency and acceptance corrections and the statistical error. In order to reach this goal the efficiency calculation has to be based on elaborate detector simulations as well as algorithms which use the data themselves. These algorithms provide not only a cross-check that the simulation is reliable but can also be used to eliminate model dependent uncertainties like the dependence of the efficiency for the selection on hadronic events of fragmentation parameters.

The luminosity is obtained from the ratio of the number of events measured in small-angle Bhabha scattering and the theoretical prediction for the cross section of this process within the acceptance of the luminosity monitor. The acceptance in polar angle of the forward detectors typically ranges from 25−120 mrad. At small polar angles the cross section for Bhabha scattering is given by :

$$\frac{d\sigma}{d\theta} \approx \frac{32\pi\alpha^2}{s}\frac{1}{\theta^3}\,.$$

A very important task of the luminosity determination is therefore the precise monitoring of the edge of the acceptance at the inner radius. If one aims at a systematic error in the permille region this requires more than a precise knowledge of the geometrical acceptance: shifts and tilts of the beam have to be considered and cuts on the energy of the scattered electrons have to be very well understood, as the energy distribution is closely linked to the acollinearity distribution. This is because Bhabha events with a photon in the initial state are boosted. Therefore the contribution of radiative corrections to the theoretical Bhabha cross section is intimately linked to the performance of the detector and the selection criteria. All experiments have upgraded their luminosity monitors after the initial successful running of LEP. They use e.g. silicon tungsten calorimeters which allow a very precise measurement of both the trajectory and the energy of the scattered electrons.

At present the experimental accuracy for the luminosity determination is better than 0.1% [14, 15, 16, 17] (to be compared with 2−5% at LEP start !). To exploit this result, a substantial effort has been invested for the calculation of higher order corrections to the theoretical Bhabha cross section. The present theoretical error amounts to 0.11% [18] and is still hoped to improve for the final LEP 1 results.

Last but not least, the precision of the centre-of-mass energy determination plays a central role for an accurate measurement of the Z^0 properties. The energy of the electrons and positrons circulating in the LEP ring is uniquely related to the magnetic field they traverse. The main contribution to the magnetic fields traversed by the beam originates from the dipole bending magnets. Electrons and positrons being highly relativistic, the length of their orbit is fixed by the radio frequency of the accelerating voltage. Changes in magnet positions cause the particles to leave their central orbits, thus receiving additional deflections in the quadrupole magnets, used for focusing. To obtain a high precision measurement of the particle energies one therefore has to consider orbit dependent corrections to the dipole field measurement.

Since 1991 LEP measures the beam energy by the resonant depolarization method, which is independent of magnetic field measurements [5]. It relies on the fact that under favourable conditions in e^+e^- storage rings transverse polarization can build up due to the interaction of the electrons or positrons with the magnetic guide field, a phenomenon referred to as the Sokolov-Ternov effect [19]. The number of spin precessions per turn, ν, is then related to the average energy, E, of the particles by:

$$\nu = \left(\frac{g-2}{2}\right)\gamma = \frac{E}{440.65\ \mathrm{MeV}}\,. \qquad (10)$$

Here g refers to the gyromagnetic constant and $\gamma = E/m_e$. Depolarization can be achieved by a weak oscillating transverse magnetic field and occurs if the frequency of the magnetic

field matches the precession frequency of the electron spins around the magnetic bending field. The intrinsic accuracy of the method is about 0.2 MeV.

The resonant depolarization technique provides an instantaneous measurement of the average energy of the particles in the ring with high accuracy which is independent of any magnetic field measurement. Orbit variations, however, constantly change the LEP energy (typically by $\mathcal{O}(1$ MeV/h)). As polarization calibrations take time (typically 2 hours) and are not possible during data taking, additional measurements (like dipole field strengths, ring temperatures and beam orbit positions) are needed and a model which relates them to energy changes. This model has been developed in 1993-94 and published [5].

For the subsequent scan in 1995 it was possible to calibrate some fills twice: once before and once after the proper data taking period. Also, the magnetic field measurement in a reference magnet was complemented by two NMR probes which were installed in two dipoles in the tunnel. These extra measurements and extra instrumentation lead to a puzzling observation: the beam energy was rising during a fill. Further observations include the following: The NMR probes showed significant noise and jumps, which were anticorrelated between the two probes at opposite sides of the ring; the rise is steepest at the beginning of a fill and the saturating; a current on the beam pipe has been measured which has a time periodicity that is correlated with the NMR probes. The resolution of this (substantially shortened) detective story was that the LEP energy calibration is also sensitive to trains (especially the French high speed TGV trains) which circulate in the Geneva area. These trains are the origin of vagabonding currents which also creep along the LEP beam pipe and modulate the magnet currents. At the beginning of a fill the magnets are still not completely in the saturation of their hysteresis curve and therefore this cycling of the magnets still contributes to a rise of the magnetic field which eventually saturates during a fill. As a result the energy determination for the 1993 and 1994 data has been revised, although studies are still in progress and the results remain preliminary.

Propagating the present preliminary errors of the energy calibration to m_{Z} and Γ_{Z} on obtains:

$$\begin{aligned} \Delta m_{\mathrm{Z}}(\text{LEP energy}) &= 1.5 \text{ MeV} \\ \Delta \Gamma_{\mathrm{Z}}(\text{LEP energy}) &= 1.7 \text{ MeV}\,. \end{aligned}$$

In the history of colliders, the precise measurement of m_{Z} and Γ_{Z} has put the most stringent requirements on the centre-of-mass energy calibration up to now. The feasibility of the resonant depolarization technique, however, was vital for the precision of several other observables at LEP.

2.1.2 Forward-backward asymmetries

Besides the total cross section one also measures the differential cross section w.r.t. the production angle. The production angle, θ, of final state fermion pair is defined as the angle between the incoming e^+ direction and the outgoing antifermion $\bar{\mathrm{f}}$ direction (Fig. 1). Theory predicts the angular distribution for the process $\mathrm{e}^+\mathrm{e}^- \to \mathrm{f}\bar{\mathrm{f}}$ to be:

$$\frac{d\sigma}{d(\cos\theta)} = 1 + \cos^2\theta + B\cos\theta \tag{11}$$

for $f \neq e$. A more complicated expression results for $f = e$ due to the presence of the t-channel process (see e.g. [20] for a parametrization of the differential cross section). Having verified that the data follow the theoretical prediction, the information content of the angular distribution can be summarized in a single number, the 'forward-backward asymmetry', A_{FB}, given by:

$$A_{FB} = \frac{N_F - N_B}{N_F + N_B} = \frac{3}{8} B \ . \tag{12}$$

Here the number of 'forward' events (N_F) is defined to be the number of events for which $\theta < \frac{\pi}{2}$. Similarly, N_B is the number of events for which $\frac{\pi}{2} < \theta < \pi$.

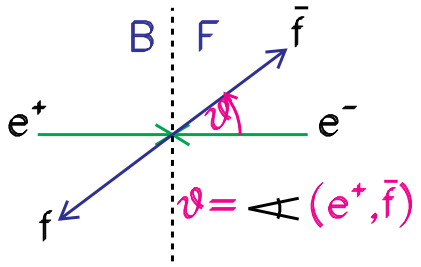

Figure 1: Definition of the scattering angle in e^+e^- collisions.

2.1.3 Parametrization of results

Before presenting the results, a word has to be said on the parametrization of cross sections and asymmetries. In the Minimal Standard Model with one isospin doublet of complex Higgs fields the lowest order predictions for the process $e^+e^- \to f\bar{f}$ can be described, neglecting fermion masses, with only 3 free parameters, which have to be determined from measurements. These 3 free parameters are usually expressed in terms quantities which are measured with the highest accuracy. The parameters most commonly used are:

$$\alpha, \ G_F \text{ and } m_Z \ , \tag{13}$$

where α is the electromagnetic coupling constant and G_F the Fermi constant.
For the process $e^+e^- \to f\bar{f}$ with $f \neq e$ the total cross section in the vicinity of $\sqrt{s} = m_Z$ is dominated by Z^0 exchange. At Born level the cross section can therefore be written as:

$$\sigma(s) = \sigma^0_{f\bar{f}} \frac{s\Gamma_Z^2}{(s - m_Z^2)^2 + \frac{s^2}{m_Z^2}\Gamma_Z^2} \ + \ \gamma Z^0 \ + \ \gamma \tag{14}$$

where $\sigma^0_{f\bar{f}}$ represents the cross section for the process $e^+e^- \to f\bar{f}$ at $\sqrt{s} = m_Z$ due to Z^0 exchange, 'γ' and 'γZ^0' represent small $\mathcal{O}(1\%)$ contributions from photon exchange and the γZ^0-interference. The pole cross section, $\sigma^0_{f\bar{f}}$, can be written in terms of the Z^0 partial decay widths into e^+e^- and $f\bar{f}$ final states, Γ_{ee} and $\Gamma_{f\bar{f}}$:

$$\sigma^0_{ff} = \frac{12\pi}{m_Z^2} \frac{\Gamma_{ee}\Gamma_{f\bar{f}}}{\Gamma_Z^2} \ . \tag{15}$$

In the Standard Model the partial widths of the Z^0 are not free parameters but can be written in terms of vector and axial vector coupling constants of the Z^0, g_{Vf} and g_{Af}:

$$\Gamma_{f\bar{f}} = \frac{G_F m_Z^3}{6\pi\sqrt{2}} \left[(g_{Af})^2 + (g_{Vf})^2 \right] . \tag{16}$$

At the tree level the couplings can be expressed as:

$$g_{Af} = \sqrt{\rho} I_f^3 \tag{17}$$

$$g_{Vf} = \sqrt{\rho}(I_f^3 + 2Q_f \sin^2\theta_W) \tag{18}$$

with:

$$\sin^2\theta_W \cos^2\theta_W = \frac{\pi\alpha}{G_F\sqrt{2}} \frac{1}{\rho m_Z^2} . \tag{19}$$

Here θ_W represents the electroweak mixing angle, Q_f and I_f^3 the charge and the weak isospin of the fermion f, respectively. The value of the ρ parameter, which measures the relative strength of neutral and charged currents, is determined by the Higgs structure of the theory. In the Minimal Standard Model, which we assume when referring to the Standard Model in the following, $\rho = 1$ at the tree level.

Also forward-backward asymmetries can be expressed in terms of vector and axial vector couplings of the Z^0. Neglecting contributions from photon exchange and the γZ^0-interference, a very simple expression is obtained for $s = m_Z^2$:

$$A_{FB}^f(s = m_Z^2) \approx A_{FB}^{0,f} \equiv \frac{3}{4} \mathcal{A}_e \mathcal{A}_f \tag{20}$$

with:

$$\mathcal{A}_f = \frac{2 g_{Vf} g_{Af}}{g_{Vf}^2 + g_{Af}^2} . \tag{21}$$

As precision measurements of the electroweak interactions aim at a test of the theory at the level of quantum corrections, the discussion of the parametrization would be incomplete without a word on radiative corrections. Here I just can point out the salient features, those interested in a more thorough introduction I would like to refer to e.g. [21], a detailed report on the state of the art can be found in [22]. Radiative corrections modify the relations introduced above. By a convention, which is rigorous only to $\mathcal{O}(\alpha)$ but sufficient to understand the basic concepts, they are separated into 3 classes, as indicated in Fig. 2:

a) Photonic corrections:

The term photonic corrections refers to all diagrams with real or virtual photons added to the Born diagram. These corrections are large ($\mathcal{O}(30\%)$) and depend on experimental cuts. The dominant contribution arises from diagrams where a photon is radiated off the initial state, thus modifying the effective centre-of-mass energy, which has a substantial effect on cross sections close to a resonance. Photonic corrections are taken into account by convoluting the cross section of the hard scattering process (c.f. eqn. (14)) by a radiator function, which can be calculated within the framework of QED.

b) Non-photonic corrections:

Non-photonic corrections denote the electroweak complement to photonic corrections.

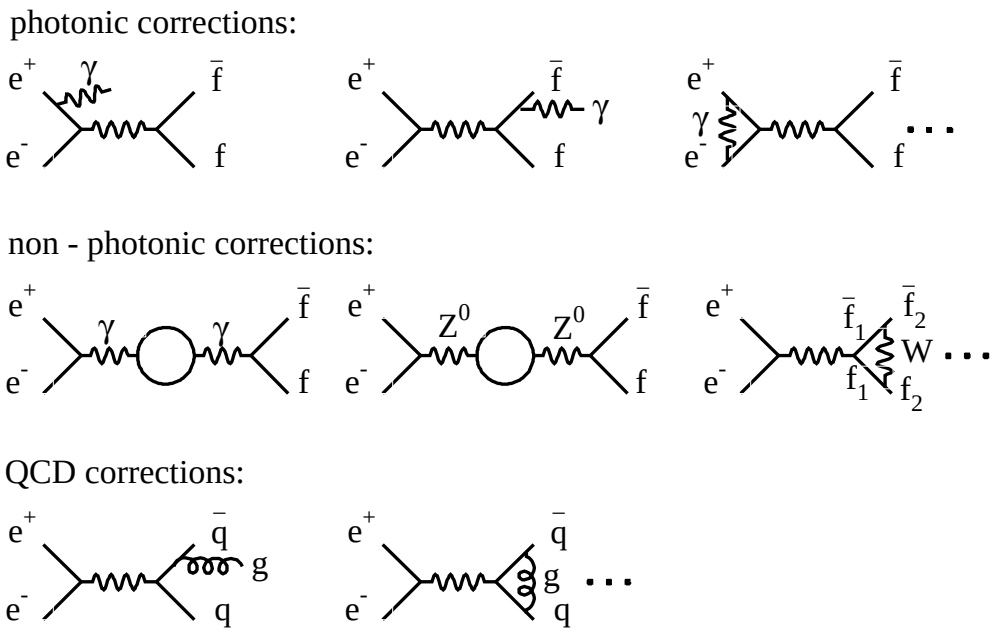

Figure 2: Radiative corrections for $e^+e^- \to f\bar{f}$.

A familiar example of non-photonic diagrams is the vacuum-polarization of the photon, which leads to an s-dependent correction of the electromagnetic coupling constant:

$$\alpha \to \alpha(s) = \frac{\alpha}{1 - \Delta\alpha(s)}$$

In the electroweak theory we have to take into account besides the photon vacuum polarization similar corrections related to Z^0-exchange and additional diagrams involving heavy gauge bosons. In pure QED a precise measurement of radiative corrections would never give us any hint of particles which have a mass far above the energy scale of the process under consideration. This is a consequence of exact charge conservation, as the associated symmetry results in a suppression of heavy physics appearing in internal loops. The electroweak symmetry is broken, however, and therefore radiative corrections involving heavy particles may have observable consequences. This is one of the most interesting aspects of electroweak radiative corrections and electroweak precision tests: They potentially probe the complete particle spectrum and not only the part which is accessible at a given energy scale.

A convenient way to take into account non-photonic radiative corrections at Z^0 energies is the improved Born approximation [23]: It requires besides the substitution $\alpha \to \alpha(m_Z)$ the introduction of effective vector and axial vector couplings. These effective couplings exhibit an s-dependence, which is, however, negligible in the vicinity of the Z^0 peak. They can still be calculated using the relations (17)−(19), but then ρ and $\sin^2\theta_W$ have to be replaced by effective parameters:

$$\sin^2\theta^f_{\rm eff} = \sin^2\theta^{\rm lept}_{\rm eff} + \Delta^f_v \qquad (22)$$

$$\rho_f = \rho_{\rm lept} + \delta^f_v\,. \qquad (23)$$

The calculation of $\sin^2\theta^{\rm f}_{\rm eff}$ depends not only on the Born parameters, α, $G_{\rm F}$ and $m_{\rm Z}$ (as implied by eqn. (19)), but also on $m_{\rm H}$ and $m_{\rm t}$. Also due to radiative corrections, $\rho_{\rm f}$ will slightly differ from 1. The fermion dependence of $\sin^2\theta^{\rm f}_{\rm eff}$ and $\rho_{\rm f}$ is due to vertex corrections, which are non-universal. The difference to leptonic vertex corrections is denoted as $\Delta^{\rm f}_v$ and $\delta^{\rm f}_v$ for $\sin^2\theta^{\rm f}_{\rm eff}$ and $\rho_{\rm f}$, respectively. For all fermions except for b quarks, $\Delta^{\rm f}_v$ and $\delta^{\rm f}_v$ are small and essentially independent of $m_{\rm t}$. Lepton asymmetries measure the ratio of couplings $g_{V\ell}/g_{A\ell}$ and can be expressed by a single parameter:

$$\sin^2\theta^{\rm lept}_{\rm eff} = \frac{1}{4}\left(1 - g_{V\ell}/g_{A\ell}\right) . \tag{24}$$

As $\mathcal{A}_{\rm e}$ is much smaller than $\mathcal{A}_{\rm q}$ the quark forward-backward asymmetries also determine $\sin^2\theta^{\rm lept}_{\rm eff}$ with very little dependence on electroweak corrections particular to the $\rm q\overline{q}$ vertex.

c) QCD Corrections:

QCD corrections to the process $\rm e^+e^- \to f\overline{f}$ account for gluon radiation off real and virtual quarks. Their dominant effect is to modify the $\rm q\overline{q}$ final state, thus affecting the $\rm Z^0$ partial widths for decays into $\rm q\overline{q}$-pairs, $\Gamma_{\rm q\overline{q}}$, and the forward-backward asymmetry, $A^{\rm q\overline{q}}_{\rm FB}$, of the reaction $\rm e^+e^- \to q\overline{q}$. The experimental precision achieved, however, also requires to take into account QCD corrections to internal quark loops.

2.1.4 Results

For the parametrization of the $\rm Z^0$ line shape and lepton forward-backward asymmetries the LEP experiments use a standard parameter set [24]:

- The mass of the $\rm Z^0$, $m_{\rm Z}$, and the total width, $\Gamma_{\rm Z}$, where the definition is based on the Breit Wigner denominator $(s - m^2_{\rm Z} + is\Gamma_{\rm Z}/m_{\rm Z})$.
- The hadronic pole cross section, $\sigma^0_{\rm h}$ (cf. eqn. (15))
- The ratios:

  $$R_{\rm e} \equiv \Gamma_{\rm had}/\Gamma_{\rm ee} \qquad R_\mu \equiv \Gamma_{\rm had}/\Gamma_{\mu\mu} \qquad R_\tau \equiv \Gamma_{\rm had}/\Gamma_{\tau\tau} .$$

  Here $\Gamma_{\mu\mu}$ and $\Gamma_{\tau\tau}$ are the partial widths of the $\rm Z^0$ for the decays $\rm Z \to \mu^+\mu^-$ and $\rm Z \to \tau^+\tau^-$.
- The pole asymmetries, $A^{0,\,\rm e}_{\rm FB}$, $A^{0,\,\mu}_{\rm FB}$ and $A^{0,\,\tau}_{\rm FB}$ for the processes $\rm e^+e^- \to e^+e^-$, $\rm e^+e^- \to \mu^+\mu^-$ and $\rm e^+e^- \to \tau^+\tau^-$ (cf. eqn. (20)).

As discussed above the mass of the $\rm Z^0$ is an important parameter to make the Standard Model predictive. Fig. 3 displays the preliminary results of the four LEP experiments and the average, which has been computed as described in [25]. Once $m_{\rm Z}$ is obtained any further measurement can be calculated, modulo uncertainties in parameters which enter via radiative corrections. This is illustrated in Fig. 4 which shows the preliminary results for the total width of the $\rm Z^0$ in comparison to the Standard Model prediction as function of $m_{\rm t}$. The width of the Standard Model band represents the uncertainties due to the error in the determination of $\alpha_s(m^2_{\rm Z})$ and the ignorance of $m_{\rm H}$.

Figure 5 shows the 68% confidence level contours in the $A^{0,\,\ell}_{\rm FB}$-R_ℓ plane. The data are consistent with lepton universality. This assumption can be used to combine the set of 9 parameters into a set of 5 parameters:

$$m_{\rm Z},\ \Gamma_{\rm Z},\ \sigma^0_{\rm h},\ R_\ell,\ A^{0,\,\ell}_{\rm FB} . \tag{25}$$

Here $R_\ell = \Gamma_{\rm had}/\Gamma_{\ell\ell}$, where $\Gamma_{\ell\ell}$ is defined as the partial Z^0 width for the decay into a pair of massless charged leptons. The LEP average of the parameter set (25) is given in Table 1.

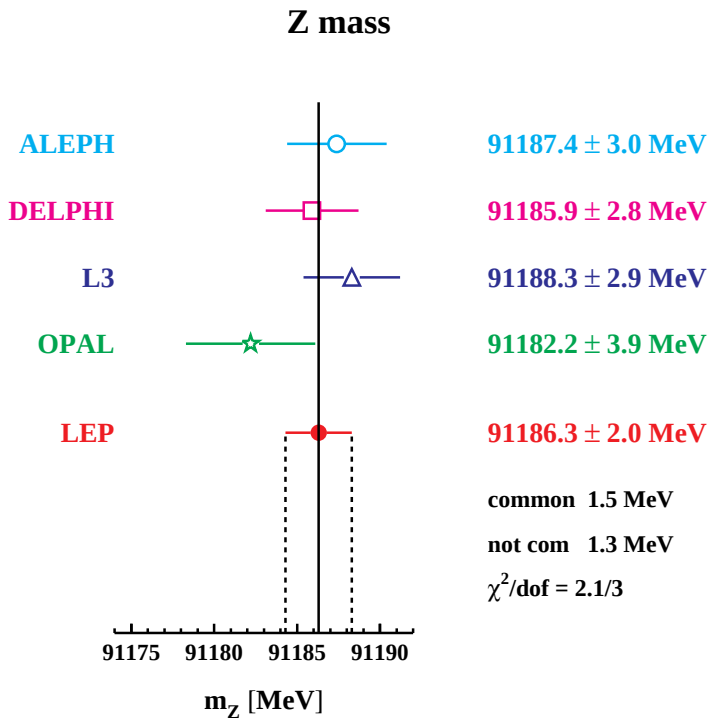

Figure 3: LEP results for $m_{\rm Z}$.

Parameter	Average Value
$m_{\rm Z}$ (GeV)	91.1863±0.0020
$\Gamma_{\rm Z}$ (GeV)	2.4946±0.0027
$\sigma^0_{\rm h}$(nb)	41.508±0.056
R_ℓ	20.778±0.029
$A^{0,\ell}_{\rm FB}$	0.0174±0.0010

Table 1: Average line shape and asymmetry parameters from the preliminary results of the four LEP experiments, assuming lepton universality [25].

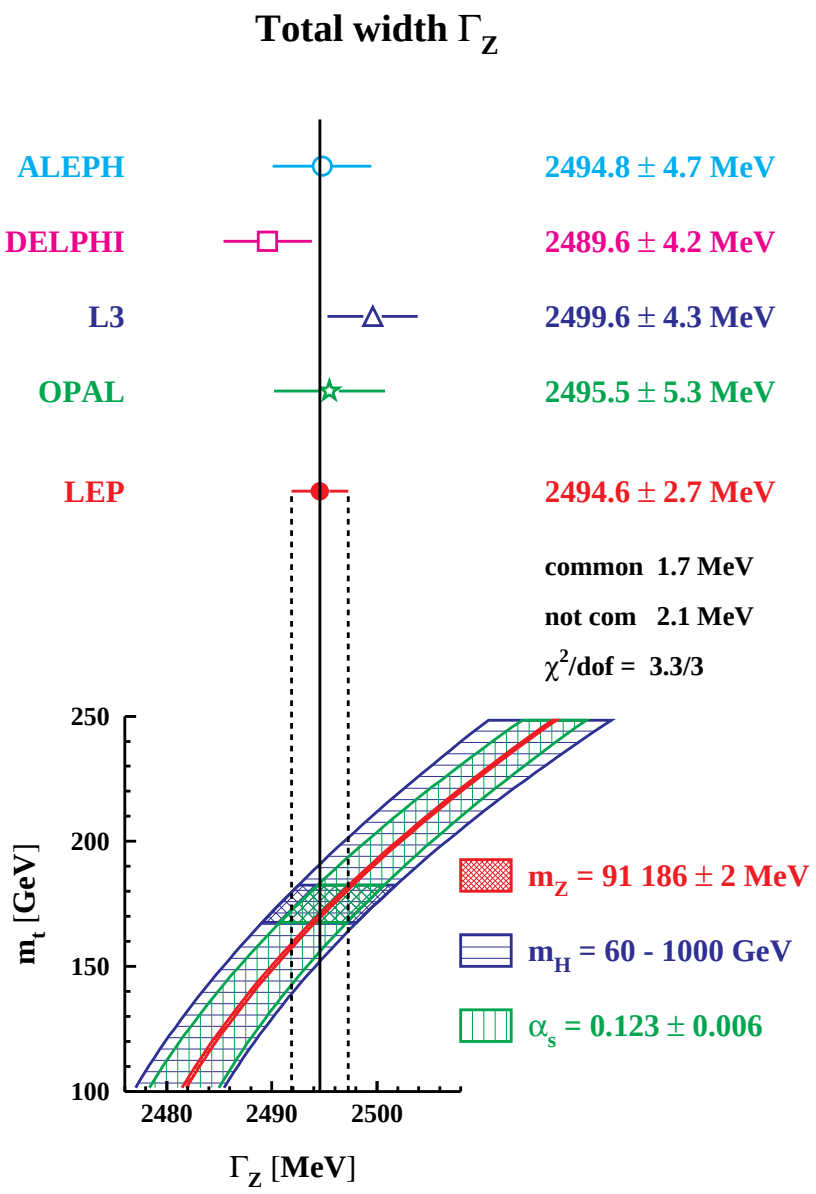

Figure 4: LEP results for Γ_Z. Also shown is the Standard Model prediction as function of m_t.

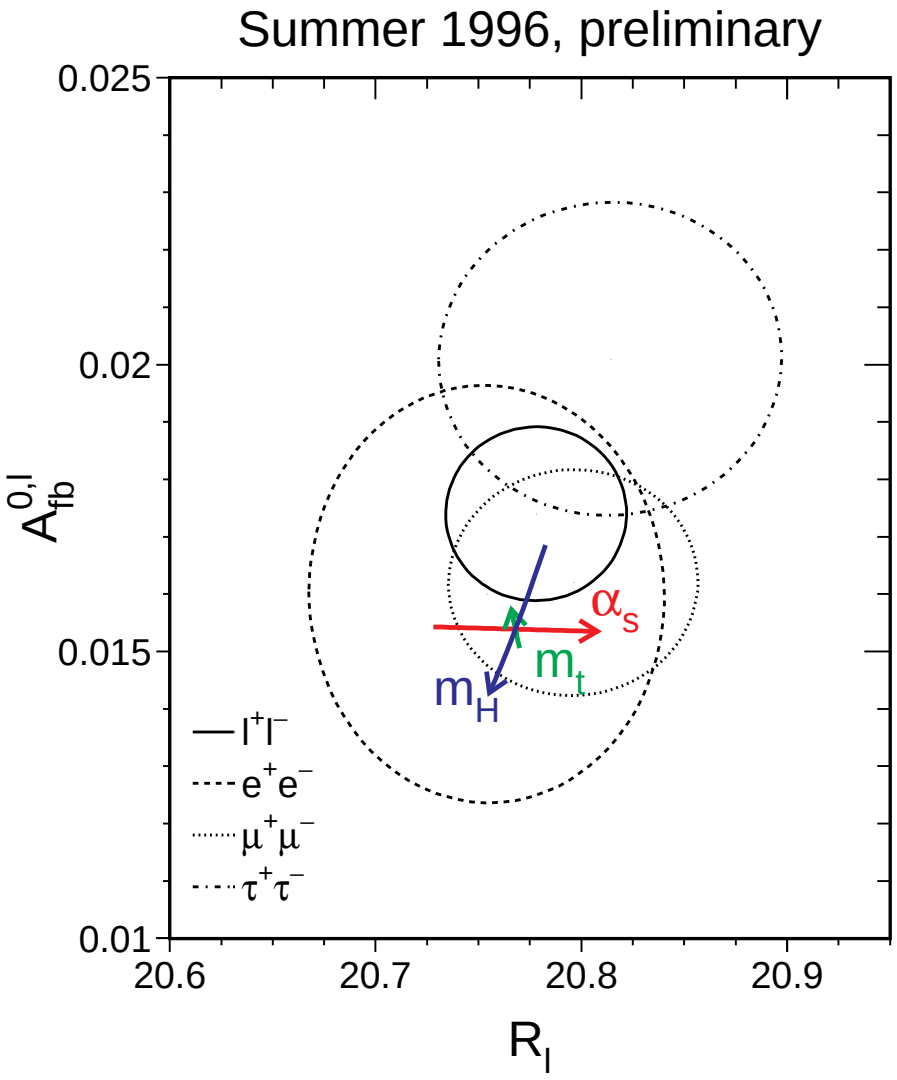

Figure 5: Contours of 68% probability in the R_ℓ-$A_{\rm FB}^{0,\ell}$ plane. The Standard Model prediction for $m_{\rm Z} = 91.1863$ GeV, $m_{\rm t} = 175$ GeV, $m_{\rm H} = 300$ GeV, and $\alpha_s(m_{\rm Z}^2) = 0.118$ is also shown. The lines with arrows correspond to the variation of the Standard Model prediction when $m_{\rm t}$, $m_{\rm H}$ or $\alpha_s(m_{\rm Z}^2)$ are varied in the intervals $m_{\rm t} = 175 \pm 6$ GeV, $m_{\rm H} = 300^{+700}_{-240}$ GeV, and $\alpha_s(m_{\rm Z}^2) = 0.118 \pm 0.003$, respectively. The arrows point in the direction of increasing values of $m_{\rm t}$, $m_{\rm H}$ and α_s.

2.2 Polarization asymmetries

The Standard Model predicts parity violation, not only for charged currents but also for neutral currents. Parity violation in neutral currents was first observed in the scattering of polarized electrons on deuterium at SLAC [26]. Parity violation in neutral currents also allows the verification of tiny effects of the γZ^0-interference in atomic transitions [27]. Today parity violation in neutral currents is well established. For the process $e^+e^- \to f\bar{f}$ it manifests itself by:

- A final state fermion polarization.
- An asymmetry of the production cross section with respect to left-handed and right-handed polarization of the incoming electron (positron) beam.

The measurement of polarization asymmetries in e^+e^- collisions at the Z^0-pole serves as a precision test of the lepton couplings.

For unpolarized e^+e^- beams the polarization $\mathcal{P}_f$ of the final state fermions is defined as:

$$\mathcal{P}_f = \frac{1}{\sigma_f^{tot}} \left(\sigma_R^f - \sigma_L^f \right) \tag{26}$$

where σ_R^f and σ_l^f refer to the production cross section of the process $e^+e^- \to f\bar{f}$ for positive and negative helicity fermions, respectively, and σ_f^{tot} denotes the total fermion production cross section. A negative value for $\mathcal{P}_f$ means that fermions produced in neutral current reactions are preferentially left-handed, as observed in charged current reactions. From an analysis of the angular distribution of the final state fermion polarization a forward-backward asymmetry $A_{FB}^{\mathcal{P}_f}$ can be defined:

$$A_{FB}^{\mathcal{P}_f} = \frac{1}{\sigma_f^{tot}} \left(\left\langle \sigma_R^f - \sigma_L^f \right\rangle_{\cos\theta>0} - \left\langle \sigma_R^f - \sigma_L^f \right\rangle_{\cos\theta<0} \right) . \tag{27}$$

Up to now the polarization of the final state fermions has only been measured for τ leptons. The τ lepton plays an exceptional role in the investigation of final state fermion polarizations in e^+e^--collisions because fermion and antifermion can easily be discriminated, the τ has a short lifetime and parity is violated in its weak decays. Assuming the $V-A$ structure of the weak charged current the decay products can therefore be used as spin analyzers. The tau decays used for this analysis are the semileptonic decays $\tau \to \pi(K)\nu$, $\tau \to \rho\nu$ and $\tau \to a_1\nu$ and the leptonic decays $\tau \to e\nu\overline{\nu}$ and $\tau \to \mu\nu\overline{\nu}$.

For polarized beams the left-right asymmetry A_{LR} is defined as:

$$A_{LR}{}^f = \frac{1}{\sigma_f^{tot}} \left(\sigma_L^f - \sigma_R^f \right) \tag{28}$$

where σ_L^f (σ_R^f) denotes the total production cross section $e^+e^- \to f\bar{f}$ for a left-handed (right-handed) polarization of the incoming electrons. From an analysis of the angular distribution of the final state fermions a polarized forward-backward asymmetry, $A_{FB}^{LR,f}$, can be derived as:

$$A_{FB}^{LR,f} = \frac{1}{\sigma_f^{tot}} \left(\left\langle \sigma_L^f - \sigma_R^f \right\rangle_{\cos\theta>0} - \left\langle \sigma_L^f - \sigma_R^f \right\rangle_{\cos\theta<0} \right) . \tag{29}$$

A precision measurement of A_{LR} has been performed at the SLAC Linear Collider with the SLD detector [28]. The source of polarized electrons is a strained GaAs photocathode which is illuminated with circularly polarized laser light. The laser polarization

is reversed randomly on a pulse by pulse basis. An elaborate spin transport system is necessary to preserve the electron polarization on their way through the damping rings, the linac and the SLC arcs to the interaction point (IP). The polarization at the IP is measured with a Compton polarimeter. The experimental determination of $A_{\rm LR}$ essentially relies on the counting of $\rm Z^0$ events, irrespective of their final state. Only events from the process $\rm e^+e^- \to e^+e^-$ have to be discarded due to the large zero asymmetry contribution from t-channel photon exchange.

The general formalism of how to include fermion helicities into the description of the differential cross section for the process $\rm e^+e^- \to f\overline{f}$ can be found in [29]. The formulae simplify considerably if only $\rm Z^0$-exchange is considered. Neglecting photonic corrections, the asymmetries defined above then have a simple relation to the vector and axial vector couplings of the $\rm Z^0$ for $s = m_{\rm Z}^2$:

$$\mathcal{P}_{\rm f}(s = m_{\rm Z}^2) = -\mathcal{A}_{\rm f} \tag{30}$$

$$A_{\rm FB}^{\mathcal{P}_{\rm f}}(s = m_{\rm Z}^2) = -\frac{3}{4}\mathcal{A}_{\rm e} \tag{31}$$

$$A_{\rm LR}(s = m_{\rm Z}^2) = \mathcal{A}_{\rm e} \tag{32}$$

$$A_{\rm FB}^{\rm LR,f}(s = m_{\rm Z}^2) = \frac{3}{4}\mathcal{A}_{\rm f}\,. \tag{33}$$

The partial widths of the $\rm Z^0$ into leptons and the lepton forward-backward asymmetries, the τ polarization asymmetries and $A_{\rm LR}$ all determine the vector and axial vector couplings for e, μ and τ. The asymmetries determine the ratio $g_{V\ell}/g_{A\ell}$ while the leptonic partial widths determine essentially the axial vector coupling squared. Figure 6 shows the 68% probability contours in the $g_{A\ell}$-$g_{V\ell}$ plane. The separate contours for electrons muons and taus are in good agreement with lepton universality and can therefore be combined.

2.3 Electroweak couplings of quarks

The determination of the effective quark couplings requires event samples with different compositions of the primary quark flavours. Up to now an exclusive separation of primary quark flavours with good purity has only been achieved for b and c quarks. For unpolarized beams the electroweak observables which are derived from the tagging of heavy flavours and the analysis of angular distributions are:

$$R_{\rm b} \equiv \Gamma_{\rm b\overline{b}}/\Gamma_{\rm had},\ R_{\rm c} \equiv \Gamma_{\rm c\overline{c}}/\Gamma_{\rm had},\ A_{\rm FB}^{\rm b\overline{b}} \text{ and } A_{\rm FB}^{\rm c\overline{c}}\,, \tag{34}$$

where $\Gamma_{\rm b\overline{b}}$ ($\Gamma_{\rm c\overline{c}}$) refers to the partial width of the $\rm Z^0$ for the decay into $\rm b\overline{b}$ ($\rm c\overline{c}$) final states and $A_{\rm FB}^{\rm b\overline{b}}$ ($A_{\rm FB}^{\rm c\overline{c}}$) to the forward-backward asymmetry of b (c) quarks. At SLC results are available for the polarized forward-backward asymmetry $A_{\rm FB}^{\rm LR,f}$ (see eqn. (29)) for b and c quarks [30] which determine $\mathcal{A}_{\rm b}$ and $\mathcal{A}_{\rm c}$ (c.f. eqn. (33)).

A meaningful comparison of heavy flavour results with the predictions of the Standard Model requires a detailed understanding of correlations and common systematics amongst the measurements. This work is also the basis for averaging the results and follows procedures [31, 25] developed by the LEP Electroweak Working Group in collaboration with representatives from the SLD Heavy Flavour Group.

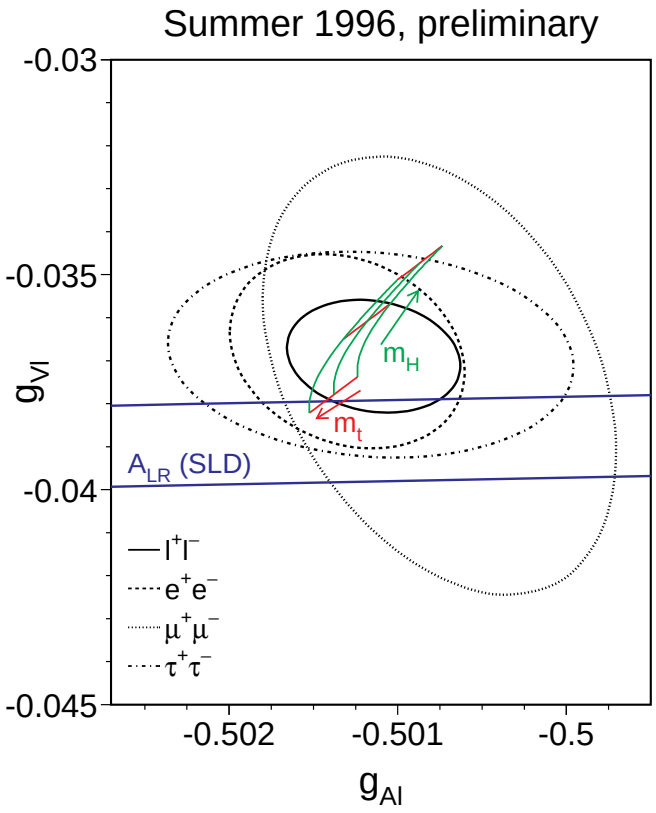

Figure 6: Contours of 68% probability in the $g_{V\ell}$-$g_{A\ell}$ plane from LEP measurements. The solid contour results from a fit assuming lepton universality. Also shown is the one standard deviation band resulting from the $A_{\rm LR}$ measurement of SLD. The shaded region corresponds to the Standard Model prediction for $m_{\rm t} = 175 \pm 6$ GeV and $m_{\rm H} = 300^{+700}_{-240}$ GeV. The arrows point in the direction of increasing values of $m_{\rm t}$ and $m_{\rm H}$.

Primary b quarks exhibit several distinct signatures: As b-flavoured hadrons are heavy, their decay products have a large p_{T} with respect to the primary B-hadron direction. Also the fragmentation of light quarks is much softer as they lose a larger fraction of their energy by gluon radiation, whereas the hadrons containing the primary b quark carry away on average about 70% of the beam energy. Furthermore B hadrons have long lifetimes, typically about 1.5 ps, resulting in decay vertices which are displaced from the main vertex by about 2 mm. These signatures lead to three b-tagging techniques: lepton tagging [32, 33, 34, 35], event shape tagging [36] and lifetime tagging [37, 38, 39, 40, 41]. The latter is today the most powerful technique, which dominates the results.

Several methods to tag events originating from primary $\mathrm{c\overline{c}}$ quarks have been used: One method is to extend the inclusive lepton analysis in the region of low p and p_{T} [32, 42, 33] where a sizable fraction of the events can be traced to primary c quarks. A complementary method to enrich a sample with $\mathrm{c\overline{c}}$ events is based on the reconstruction of fast charmed mesons [42, 43, 44]. The prototype analysis makes use of the chain:

$$c \to \mathrm{D}^* X \to \mathrm{D}^0 \pi X \to (\mathrm{K}\pi)\pi X$$

Other decay modes and tagging mesons are used.

An important analysis method for the section of b and c quarks is the double-tagging technique. For such analyses the event is divided into two hemispheres by a plane orthogonal to the thrust axis. Then the number of tagged hemispheres, N_t, and the number of events with both hemispheres tagged, N_{tt}, are counted. For their ratio to the total number of hadronic events, N_{had}, one obtains:

$$\begin{aligned} \frac{N_t}{2N_{\mathrm{had}}} &= \varepsilon_{\mathrm{b}} R_{\mathrm{b}} + \varepsilon_{\mathrm{c}} R_{\mathrm{c}} + \varepsilon_{\mathrm{uds}}(1 - R_{\mathrm{b}} - R_{\mathrm{c}}), \\ \frac{N_{tt}}{N_{\mathrm{had}}} &= \mathcal{C}_{\mathrm{b}} \varepsilon_{\mathrm{b}}^2 R_{\mathrm{b}} + \mathcal{C}_{\mathrm{c}} \varepsilon_{\mathrm{c}}^2 R_{\mathrm{c}} + \mathcal{C}_{\mathrm{uds}} \varepsilon_{\mathrm{uds}}^2 (1 - R_{\mathrm{b}} - R_{\mathrm{c}}). \end{aligned}$$

Here ε_{b}, ε_{c} and $\varepsilon_{\mathrm{uds}}$ are the tagging efficiencies per hemisphere for b, c and light-quark events, and $\mathcal{C}_{\mathrm{q}} \neq 1$ accounts for the fact that the tagging efficiencies between the hemispheres may be correlated.

In the case of methods designed to determine R_{b} one has $\varepsilon_{\mathrm{b}} \gg \varepsilon_{\mathrm{c}} \gg \varepsilon_{\mathrm{uds}}$, $\mathcal{C}_{\mathrm{b}} \approx 1$. The correlations for the other flavours can be neglected. These equations can be solved to give R_{b} and ε_{b}. Neglecting the c and uds backgrounds and the correlations they are approximately given by:

$$\begin{aligned} \varepsilon_{\mathrm{b}} &\approx 2N_{tt}/N_t, \\ R_{\mathrm{b}} &\approx N_t^2/(4N_{tt}N_{\mathrm{had}}). \end{aligned}$$

The double-tagging method has the advantage that the b tagging efficiency is derived directly from the data, reducing the systematic error of the measurement. The residual background of other flavours in the sample, and the evaluation of the correlation between the tagging efficiencies in the two hemispheres of the event are the main sources of systematic uncertainty in such an analysis.

Double tagging techniques have also been applied for the selection of primary c quarks, but here the loss in statistics is more severe, as c tagging techniques are far less efficient.

For the determination of quark forward-backward asymmetries the important task is to discriminate the jet containing the primary quark against the jet with the primary antiquark. The traditional method for $A_{\rm FB}^{\rm b\bar{b}}$ and $A_{\rm FB}^{\rm c\bar{c}}$ is restricted to the inclusive lepton sample, where the quark charge can be inferred from the lepton charge. In a similar way the charge of reconstructed $\rm D^*$ mesons can be used. To profit from the statistics of $\rm b\overline{b}$ events selected by lifetime tagging techniques not only for $R_{\rm b}$ but also for $A_{\rm FB}^{\rm b\bar{b}}$, jet charge algorithms are applied. The idea behind these algorithms is that the primary quark charge manifests itself in the fast hadrons. Therefore the primary quark charge is derived from a momentum weighted average of hadron charges in the jet.

Figure 7 shows the confidence level contours for the combined LEP results of $R_{\rm b}$ and $R_{\rm c}$. Also shown is the Standard Model prediction, which is in agreement with the data. Since summer 1995 the results for the heavy quark production rates $R_{\rm b}$ and $R_{\rm c}$ have moved towards the Standard Model prediction (see [25] for a summary of results), but the changes are understood. They can be traced to new data being analysed, new analysis techniques and the replacement of the product branching ratio $\rm P(c \to D^{*+}) \times BR(D^{*+} \to \pi^+ D^0)$ from low energy data by a consistent but more accurate (and in view of a possible energy dependence more appropriate) measurement from the LEP experiments themselves [25]. A summary of electroweak heavy flavour results from LEP and SLC can be found in Table 2.

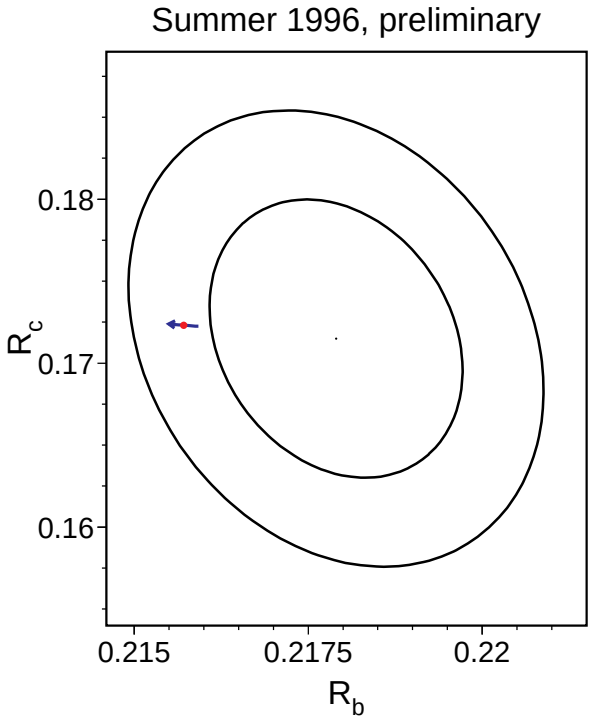

Figure 7: Contours in the $R_{\rm b}$-$R_{\rm c}$ plane derived from LEP data, corresponding to 68% and 95% confidence levels assuming Gaussian systematic errors. The Standard Model prediction for $m_{\rm t} = 175 \pm 6$ GeV is also shown. The arrow points in the direction of increasing values of $m_{\rm t}$.

$R_{\rm b}$	0.2178±0.0011
$R_{\rm c}$	0.1715±0.0056
$A_{\rm FB}^{0,\,{\rm b}}$	0.0979±0.0023
$A_{\rm FB}^{0,\,{\rm c}}$	0.0735±0.0048
$\mathcal{A}_{\rm b}$	0.863±0.049
$\mathcal{A}_{\rm c}$	0.625±0.084

Table 2: Average electroweak heavy flavour results from LEP and SLC

3. W properties and couplings

3.1 First observation of W^+W^- production in e^+e^- collisions

In June 1996 LEP 2 started operation at 161 GeV. The LEP experiments collected each ≈ 10 pb^{-1} at this energy and later in November again ≈ 10 pb^{-1} at 172 GeV. One of the important goals of LEP 2 is precision physics with W pairs.

Fig. 8 shows the Born level diagrams contributing to the process $e^+e^- \to W^+W^-$. In contrast to LEP 1 the statistics at LEP 2 is tiny. As an illustration, Table 3 lists the cross section of the process $e^+e^- \to W^+W^-$ for a few centre-of-mass energies and the number of expected events for an integrated luminosity of 500 pb^{-1} which is expected during the lifetime of LEP 2.

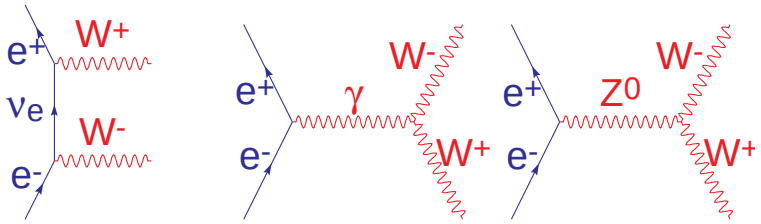

Figure 8: Born diagrams contributing to W boson pair production.

E_{CM} [GeV]	$\sigma_{\rm W^+W^-}$ [pb]	$N_{ev}/500{\rm pb}^{-1}$
161	3.6	1800
175	13.8	6900
192	17.1	8600

Table 3: W^+W^- cross sections and event rates

The event signatures for W boson pair production can be classified according to the decay mode of the individual W-bosons and are summarized in Table 4. Decay branching fractions are related by a formula based on the universality of charged current couplings:

$$Br({\rm W} \to {\rm q_i}\overline{\rm q_j}) = {\rm N_c}\delta_{\rm QCD}\delta_{\rm mass}{\rm Br}({\rm W} \to \ell\nu)\,, \tag{35}$$

where $N_c = 3$ stands for the colour factor, δ_{QCD} and δ_{mass} are small correction factors for gluon radiation and quark masses. Neglecting these corrections, the different W pair

decay topologies can be calculated as a mere counting exercise based on the number of possible final states (c.f. column 2 of Table 4). A typical hadronic 4-jet event from W boson pair production is shown in Fig. 9.

topology	Br with CC universality	Br with corrections
jjjj	'6/9× 6/9'	45.6%
jj$\ell\nu$	'2× 6/9× 3/9'	43.8%
$\ell\nu\ell\nu$	'3/9× 3/9'	10.6%

Table 4: W^+W^- event signatures and branching fractions

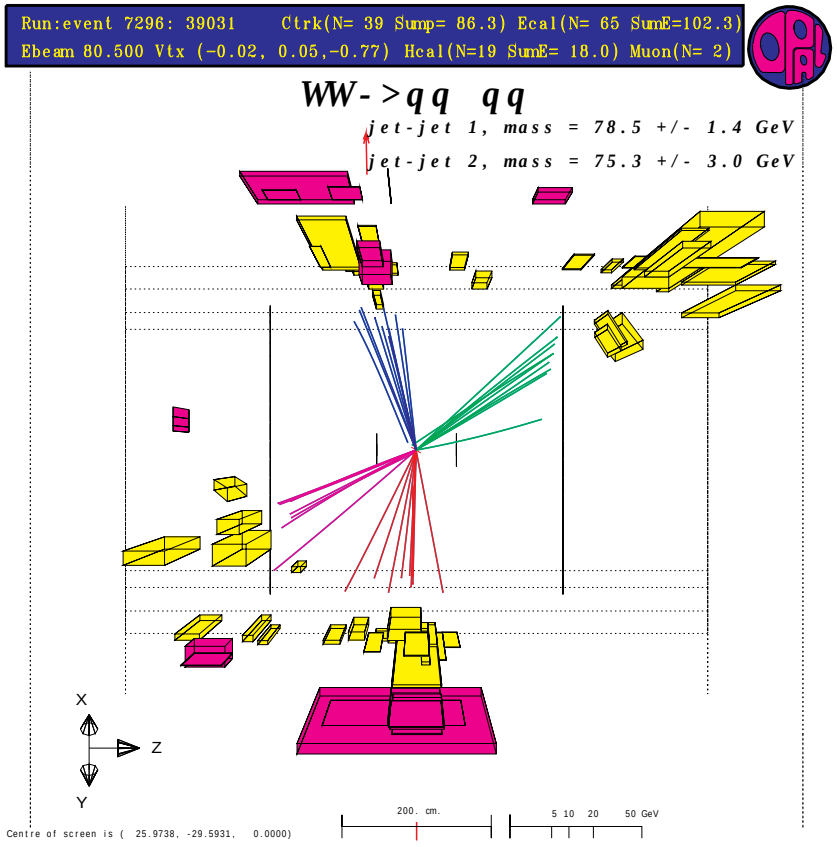

Figure 9: A typical candidate event for the process $e^+e^- \to W^+W^- \to q\bar{q}q\bar{q}$.

3.2 Determination of the mass of the W

From existing precision tests at the Z^0-pole the mass of the W can be predicted based on Standard Model relations with a precision of $\Delta m_W \approx 40$ MeV. Compared to the measurements at the Z^0-pole a different class of radiative corrections contributes to m_W and therefore a precision measurement of m_W constitutes an important test of the Standard Model. An overview of existing measurements is shown in Fig. 10.

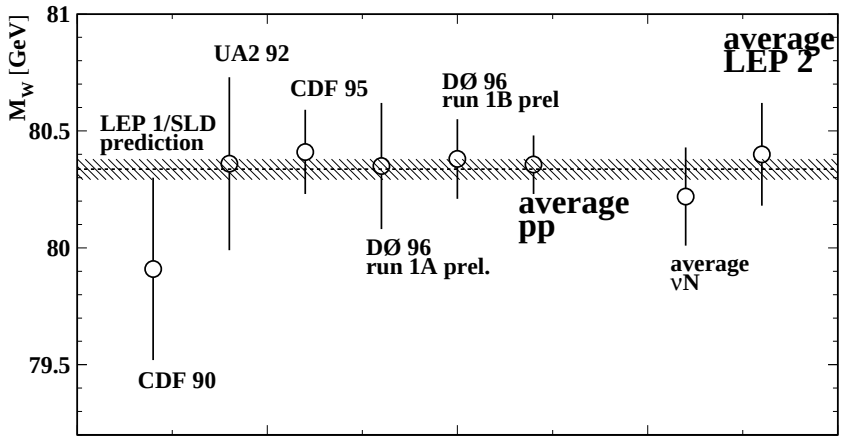

Figure 10: Status of W-mass measurements in $p\overline{p}$ collisions, νN scattering and at LEP 2.

3.2.1 m_W at $p\overline{p}$ colliders

Until summer 1996 the measurement of m_W was an exclusive domain of $p\overline{p}$ colliders. Here W boson candidates are selected using the leptonic decays $W \to \ell\nu$, where ℓ stands for either muon or electron. Due to the spectator remnants of p and $\overline{p}$ which escape along the beam pipe only the transverse components of kinematic variables can be used to constrain the event kinematics at hadron colliders. W boson candidate events are required to have a lepton with high transverse momentum, p_t^ℓ, and a high transverse missing energy, E_t^{miss}. Also required is a high reconstructed transverse mass of the W, M_t^W, which is determined from the reconstructed transverse momenta, p_t^ℓ and p_t^ν, of the charged lepton and the neutrino:

$$M_t^W = \sqrt{2p_t^\ell p_t^\nu (1 - \cos\phi(\ell,\nu))}$$

with $\cos\phi(\ell,\nu)$ being the azimuthal angle between the charged lepton and the neutrino directions. In addition there are fiducial and isolation cuts.

Important experimental aspects are the calibration of the lepton energy scale, the evaluation of backgrounds and the modeling of the transverse momentum of the hadronic recoil jet. The value of m_W is determined from a fit of the transverse mass spectrum of the reconstructed W bosons. Fig. 11 shows the transverse mass spectrum obtained by the DØ collaboration for a sample of $\approx 27\,000$ W candidates in run 1b.

The preliminary world average from direct measurements at $p\overline{p}$ colliders is [45]:

$$m_W = 80.356 \pm 0.125 \text{ GeV},$$

based on a common error of 85 MeV due to uncertainties in the proton structure functions.

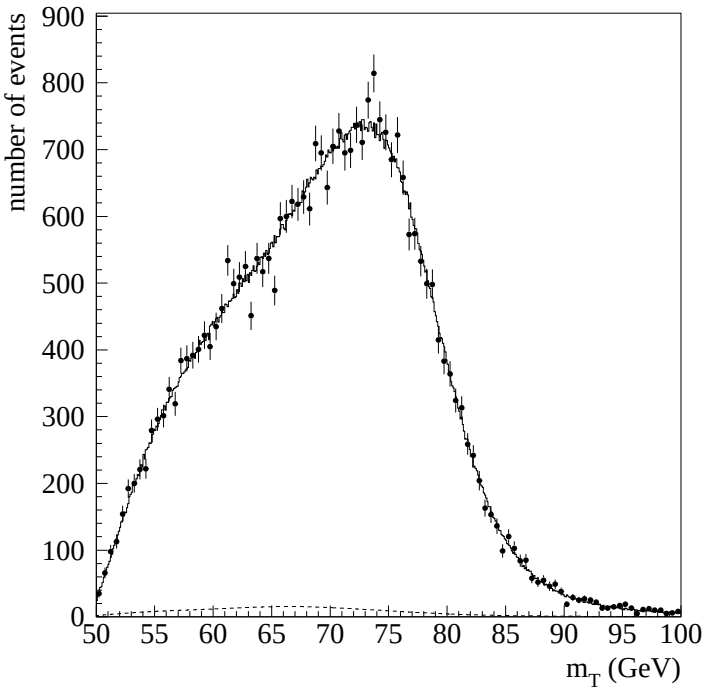

Figure 11: The transverse mass distribution for the W candidates of the DØ experiment [45, 46].

3.2.2 m_W at LEP 2

In e^+e^- collisions there are two complementary methods for the determination of m_W: the measurement of the production cross section and the direct reconstruction.

First results exist already for the method based on a measurement of the W production cross section. Fig. 12 shows the theoretical cross section $e^+e^- \to W^+W^-$ as function of centre-of-mass energy for different values of m_W. It can be seen that the difference among these cross section curves depends on centre-of-mass energy. An optimization study [47] shows that the error of m_W for fixed integrated luminosity has a relatively broad minimum at

$$\sqrt{s} = 2m_W + 0.5\ GeV\,.$$

The preliminary LEP result for m_W based on this method with the data taken at 161 GeV is displayed in Fig. 13. The error on m_W is dominated by the statistical component.

The second method in e^+e^- collisions is based on the direct reconstruction of m_W. Here the observed event topology is subject to a constrained kinematic fit. Table 5 from [47] shows the expected errors of m_W for an integrated luminosity of 500 pb^{-1}. The systematic error is dominated by components which are common to all experiments: The error in the LEP beam energy and theoretical errors. These are due to the understanding of initial state radiation, the evaluation of backgrounds and the fragmentation process. For the fully hadronic channel there is also an uncertainty referred to as 'colour interconnection'. It is due to soft gluons which connect the two hadronic systems of the decaying W bosons and therefore have an impact on the mass which is reconstructed from the observed jets. As this effect cannot be calculated perturbatively it is at present

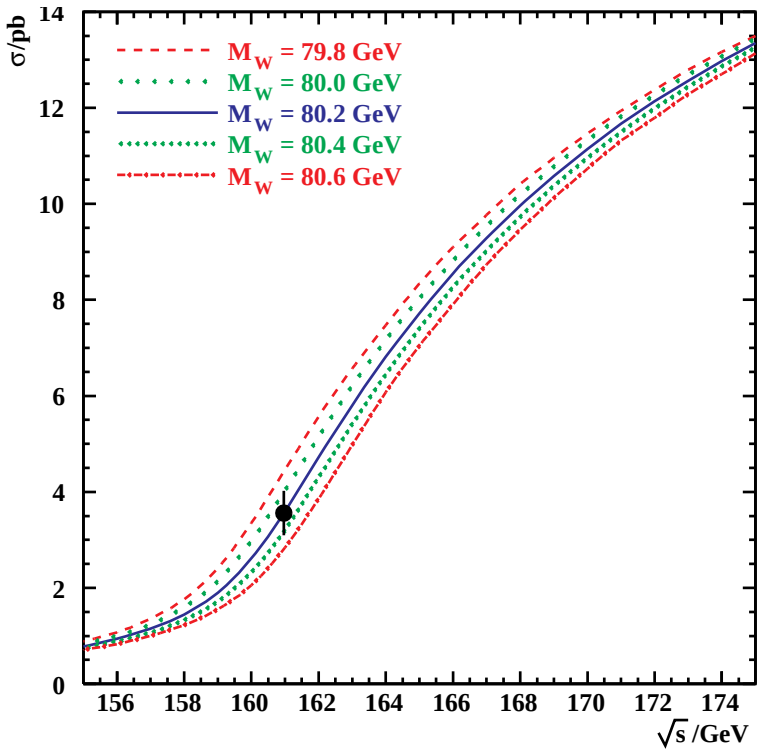

Figure 12: The cross section for the process $e^+e^- \to W^+W^-$ as function of centre-of-mass energy for different values of m_W.

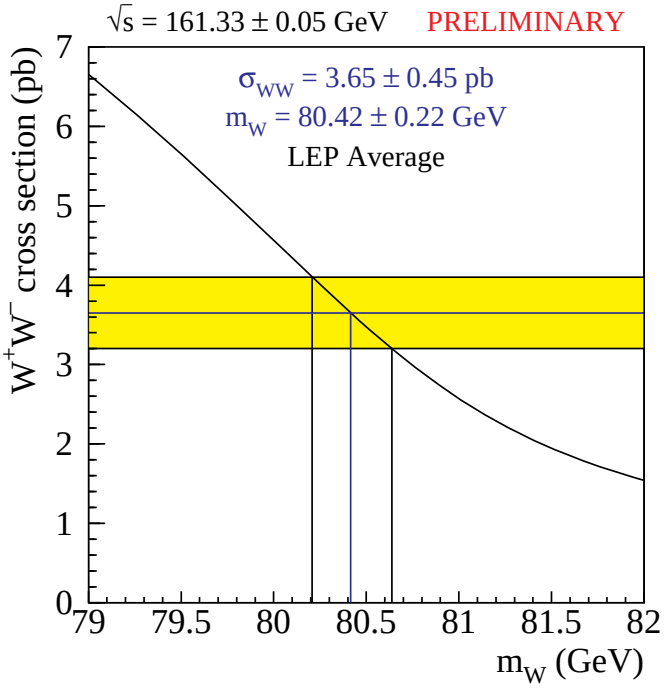

Figure 13: The cross section for the process $e^+e^- \to W^+W^-$ at a centre-of-mass energy of 161.33 GeV as function of m_W. Also indicated is the LEP average result for this cross section [48].

difficult to estimate, and we still don't know whether the fully hadronic channel can be used at all. It is hoped, however, that the data themselves will provide an estimate of the size of this effect (similarly to LEP 1, where the data imposed considerable constraints on fragmentation models).

Source	$W^+W^- \to q\bar{q}q\bar{q}$	$W^+W^- \to q\bar{q}\ell\nu$	Combined
Statistical	36	36	25
Common systematic	25	23	23
Uncorr. systematic	9	9	6
Total	45	44	34

Table 5: Expected accuracy of m_W in MeV for the direct reconstruction method based on an integrated luminosity of 500 pb^{-1} delivered by LEP 2. The numbers refer to an average of the four experiments; the yet uncertain effect of colour interconnection for the $W^+W^- \to q\bar{q}q\bar{q}$ channel is not included in the common systematics quoted.

The sensitivity of the direct reconstruction method is comparable to the threshold cross section measurement and not very sensitive to a variation in energy above 170 GeV. Depending on the question whether the 4-jet channel can be used an error of the LEP average $\Delta m_W = 30 - 40$ MeV is expected for an integrated luminosity of 500 pb^{-1}.

3.3 Anomalous W couplings

The only allowed trilinear gauge coupling in the Standard Model are the γWW and ZWW vertices. Other couplings may occur in extensions of the Standard Model. In the Standard Model strong gauge cancellations, e.g. among the amplitudes in Fig. 8 ensure unitarity for production cross-sections. For anomalous couplings unitarity has to be restored by introducing new physics at some higher energy scale, parametrized by the introduction of generalized dipole form factors.

A signature of anomalous couplings at the Tevatron is an excess of diboson production. The Tevatron analysis is in agreement with the Standard Model expectation, a discussion of recent bounds on anomalous couplings can be found in [49].

At LEP 2 anomalous couplings [50] can be detected in the distribution of the W pair production angle. By analysing the angular distributions of the W decay products it will also be possible to include the W helicities in the analysis, strengthening the tests for anomalous couplings. LEP 2 is expected to improve existing limits by a factor 5−10.

4. Measurement of α_s

A tremendous amount of contributions to our understanding of QCD originate from colliders, covering both perturbative and non-perturbative aspects. In these lectures I will discuss only the determination of the strong coupling constant α_s, as QCD is a theory which can be made predictive with a single measurement.

An important aspect of the theory is that α_s has a dependence on the momentum transfer, Q, which to first order is given by:

$$\alpha_s(Q^2) = \frac{1}{\beta_0 \ln \frac{Q^2}{\Lambda^2_{\overline{MS}}}} (1 + ...) \ . \tag{36}$$

Here $\Lambda_{\overline{MS}}$ represents a scale parameter with the dimension of an energy. The strength of the Q^2 dependence is given to first order by $\beta_0 = (11 - \frac{2}{3}N_F)/(4\pi)$ which depends on the number of quark flavours N_F with masses less than momentum transfer Q. The value of α_s decreases with energy, an important feature of QCD referred to as asymptotic freedom. At high energies the value of α_s becomes sufficiently small to allow perturbative calculations of experimental observables.

For the determination of α_s a great variety of observables can be used which are sensitive to hard gluon radiation. As a QCD prediction is needed for the derivation of α_s from the measurement, the observables chosen have to be infrared and collinear stable, i.e. must not change abruptly if a soft parton is added to the event configuration or if a parton is split into two collinear ones.

It is beyond the scope of these lectures to cover the full span of α_s measurements at colliders which include:

- $R_\ell = \Gamma_{\mathrm{had}}/\Gamma_{\ell\ell}$
- $R_\tau = Br(\mathrm{e^+e^-} \to \mathrm{hadrons})/\mathrm{Br}(\mathrm{e^+e^-} \to \ell^+\ell^-)$
- jet rates
- event topologies
- scaling violations
- bound states of heavy quarks
- photoproduction

and I would like to refer the interested reader to review articles in the literature [51, 52].

Instead I will discuss one measurement as an example: jet rates in ep collisions. This rather recent result belongs to the interesting class of α_s measurements which simultaneously probe the value and the energy dependence of the strong coupling constant. Here one considers the rate of events in ep collisions with 1 jet and 1 spectator jet from the proton remnant ('1+1', Fig. 14a)) as compared to the rate of events with 2 jets and 1 spectator jet('2+1', Fig. 14b)). The momentum transfer of these events Q^2 can be evaluated from the kinematics of the scattered electron. Fig. 15 shows the measured jet rates for the ZEUS experiment for different intervals of Q^2 [53], a similar result is available from the H1 experiment [54]. At present the significance of the Q^2 dependence of α_s is still limited by statistics. Combining the measurements at all Q^2 values, the dominant systematic error is due to missing higher order calculations (which leads to an uncertainty referred to as 'scale uncertainty' in QCD studies).

Fig. 16 shows a world summary for all available measurements of α_s as function of Q^2. Using relation (36) extended to third order and accounting for heavy flavour thresholds modifying N_F, the α_s measurements at different Q^2 values can be translated to $\alpha_s(Q^2 = m_{\mathrm{Z}}^2)$ as shown in Fig. 17. The agreement of results within the error bars quoted is striking (the $\chi^2/d.o.f.$ of a simple weighted average is significantly better than one), but this is no surprise as the error of most of these measurements is dominated by theoretical uncertainties and some of them are known to be correlated.

As not all correlations can be evaluated precisely and theoretical errors are in general non-Gaussian, the averaging of α_s measurements is a problem. There are recipes but no principles how to deal with this situation. Whatever recipe is used, however, to perform an average the mean value is extremely stable [55]: $\overline{\alpha_s(m_{\mathrm{Z}}^2)} = 0.118$. The error of the mean value depends of course on the procedure used and covers the range

$\Delta\overline{\alpha_s(m_Z^2)} = 0.002 - 0.006$. The shaded band in Fig. 17 refers to $\overline{\alpha_s(m_Z^2)} = 0.118 \pm 0.006$. The error chosen in [55] is based on counting the relative number of measurements with central values within $\pm\Delta\overline{\alpha_s(m_Z^2)}$ around the mean value. The interval containing 90% of the measurements is advocated as a pragmatic and safe error estimate in view of known and unknown correlations and probability density functions.

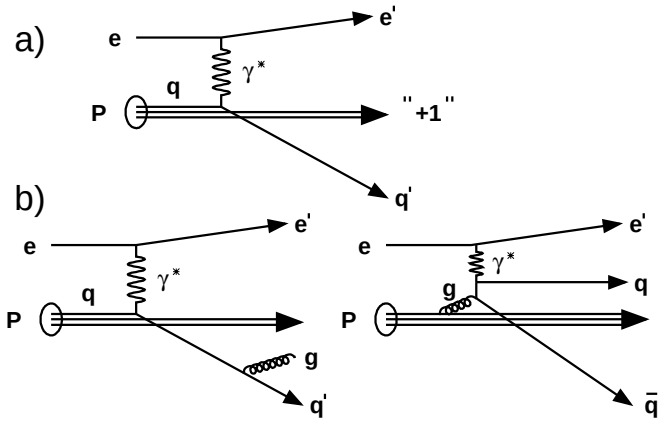

Figure 14: Diagrams contributing to a) the '1+1' and b) the '2+1' jet rate in ep collisions.

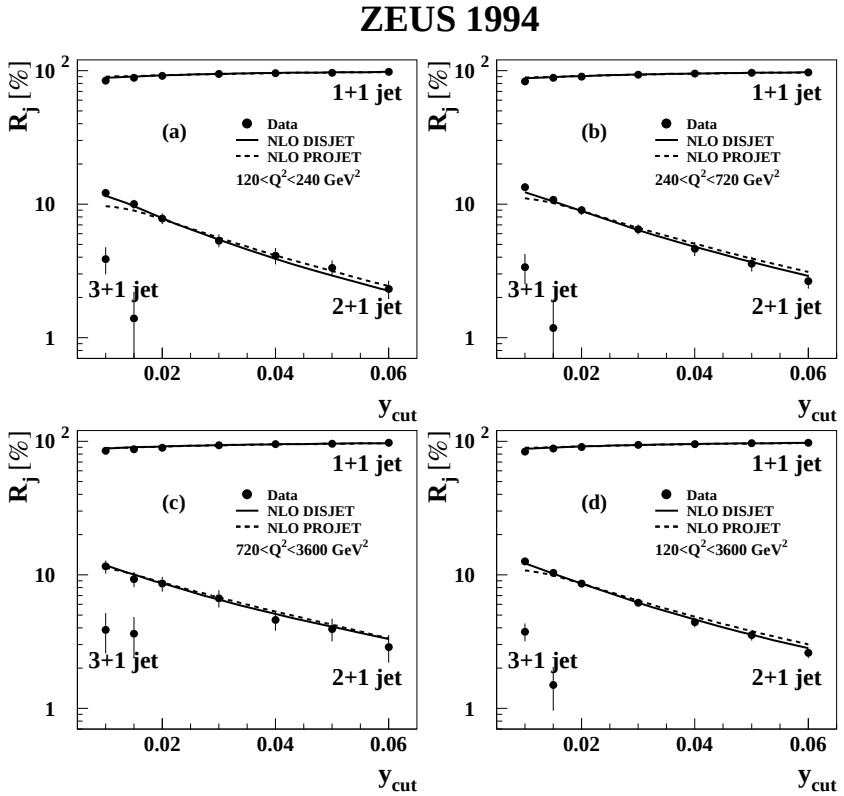

Figure 15: Jet production rates R_j as a function of the jet resolution parameter y_{cut} (from [53]) for Q^2 in the range (a) $120 < Q^2 < 240$ GeV^2, (b) $240 < Q^2 < 720$ GeV^2, (c) $720 < Q^2 < 3600$ GeV^2, and (d) $120 < Q^2 < 3600$ GeV^2. Only statistical errors are shown. The comparison with two QCD calculations (next to leading order; DISJET and PROJET) is also shown.

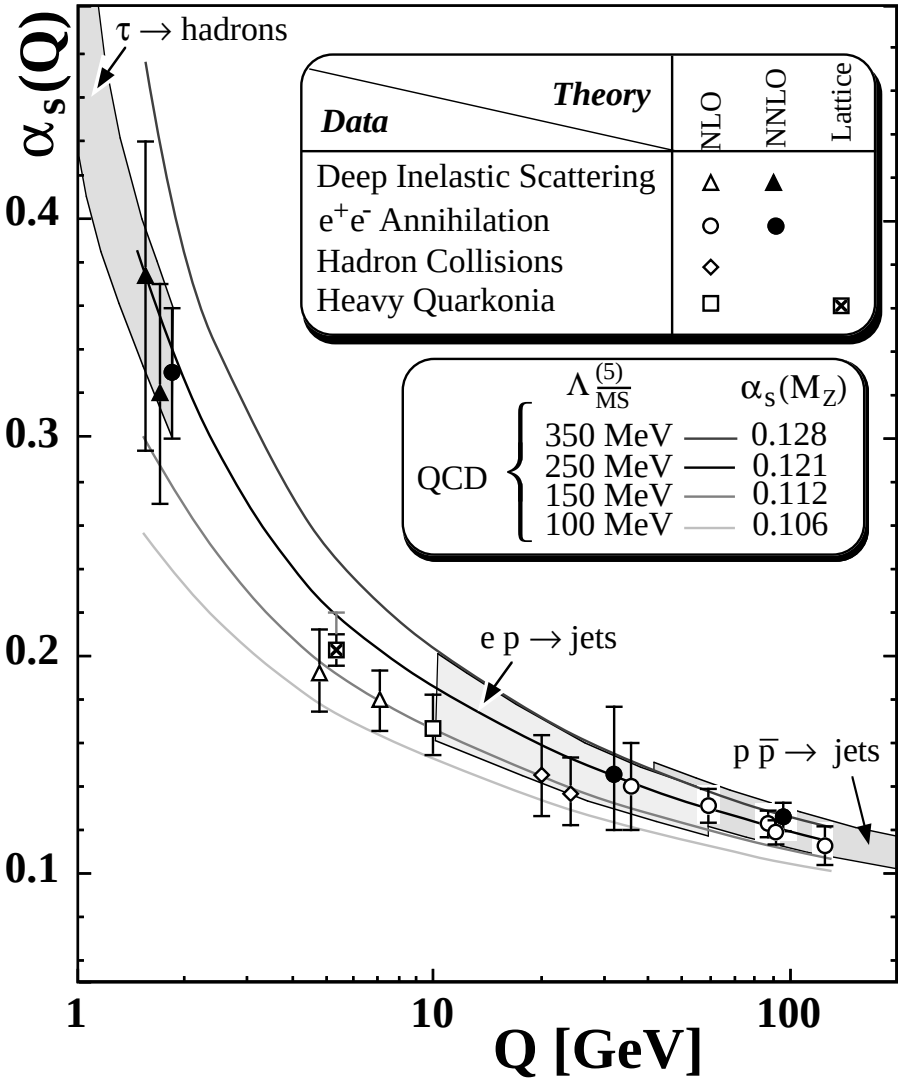

Figure 16: Summary of $\alpha_s(Q^2)$ measurements and the comparison with the QCD prediction for 4 different values of $\Lambda_{\overline{MS}}$ (from [55]).

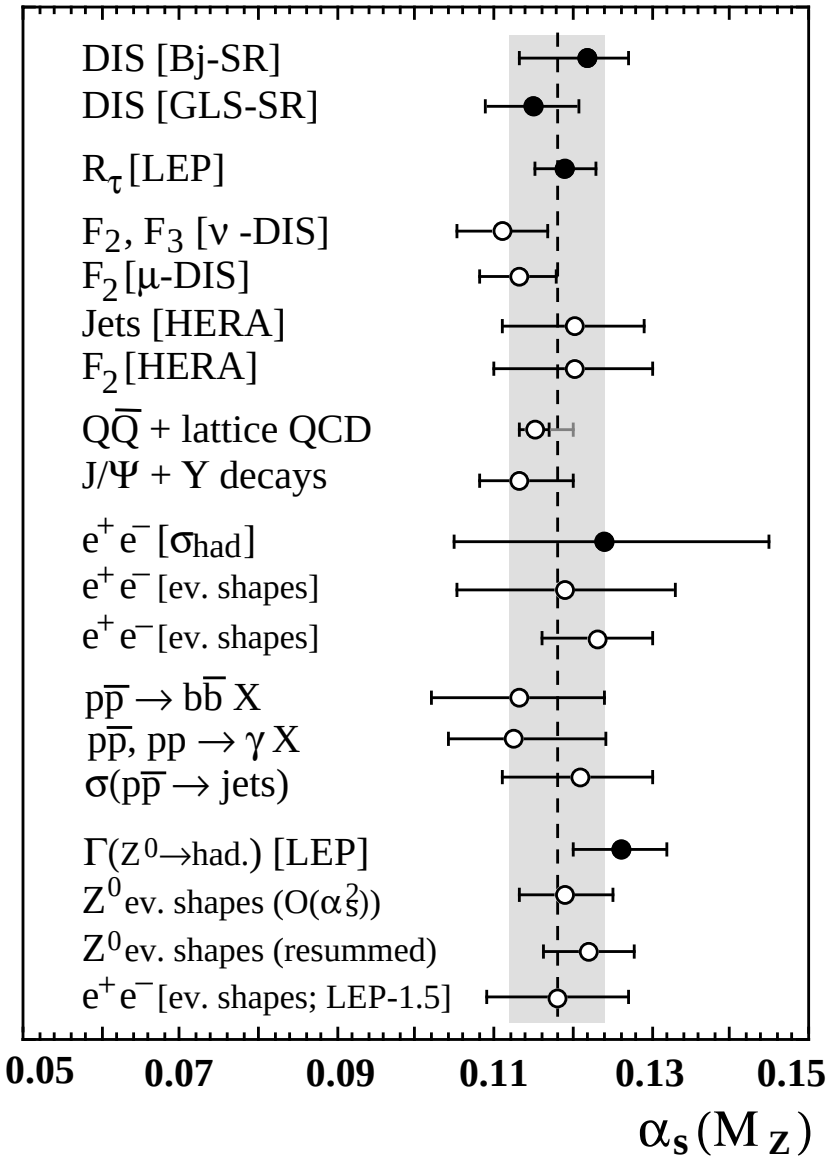

Figure 17: The value of $\alpha_s(m_Z^2)$ derived from a summary of measurements at different momentum transfers. Filled symbols refer to results obtained with an $\mathcal{O}(\alpha_s^3)$ calculation (from [55]).

5. Observation of the top quark

Since the discovery of the b quark in 1977 [56] the search for its isospin partner, the top quark, had a tremendous impact on the research program of colliders. Already in 1984, the UA1 collaboration reported on the 'Associated production of an isolated large transverse momentum lepton (electron or muon), and two jets at the CERN $p\overline{p}$ collider' which they stated to be inconsistent with known processes including 5 quark flavours but could well be explained by the hypothesis that they originate from the decay $W \to \overline{t}b$ [57]. A top quark in the inferred mass range would have been observed at LEP 1. In the years 1984−1994, however, this interpretation was superceeded by exclusion limits for m_t which were climbing well beyond the reach of LEP 2. In 1994 the CDF collaboration finally claimed 'Evidence for Top Quark Production in $p\overline{p}$ collisions at $\sqrt{s} = 1.8$ TeV' [58]. The inferred mass of $m_t = 174 \pm 10^{+13}_{-12}$ GeV was in good agreement with the value of m_t predicted from electroweak precision tests [24]. Nonetheless the lack of statistics at that time prevented them from formally claiming the discovery of top. This changed after a further year of successful running of the Tevatron when both, the CDF and the DØ collaboration, published on 'the Observation of Top' [59, 60].

The dominant mechanisms leading to the production of top quarks in the observed mass range are shown in Fig. 18. The $q\overline{q}$ annihilation into a gluon which subsequently splits into a $t\overline{t}$ pair accounts for $\approx 90\%$ of the production cross-section. Assuming the Standard Model and current limits on the CKM matrix the top quark decays to nearly 100% by the decay into an on-shell W boson and a b quark.

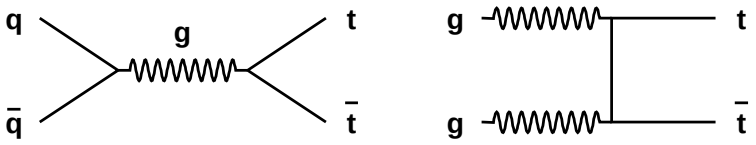

Figure 18: The dominant production mechanisms for high mass top quarks in $p\overline{p}$ collisions.

For the analysis one discriminates three event classes:

– The dilepton channel.
  The analysis is sensitive to events with both top quarks decaying via $t \to Wb \to \ell\nu b$. It requires two isolated leptons (e or μ) with opposite charge and large transverse momentum which should have an invariant mass distinct from m_Z, large transverse missing energy and ≥ 2 jets.
– The lepton+jets channel.
  The analysis is sensitive to events with one top quark decaying via $t \to Wb \to \ell\nu b$ and the other via $t \to Wb \to q_i\overline{q}_j b$. It requires one isolated lepton (e or μ) with high transverse momentum, missing transverse energy and ≥ 4 jets. This signature is, however, not yet strong enough to discriminate against the dominant background arising from the reaction $p\overline{p} \to W + jets$ (s. Fig. 19). To improve the signal to background ratio one requires that either one of the jets is explicitly tagged as b-jet via a lepton or a lifetime tag or one imposes a set of kinematical cuts involving e.g. aplanarity and the H_T variable defined as the sum of the transverse energy of the jets.

– The all hadronic channel.
This channel is particularly difficult because of the overwhelming QCD multijet background. The criteria involve both kinematical cuts and b quark tagging.

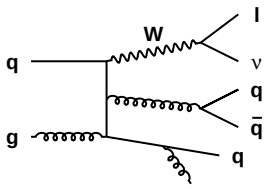

Figure 19: The dominant background in the $t\bar{t}$ candidate sample in the 'lepton+jets' channel before b-tagging.

With this selection both experiments obtain cross sections which are in agreement with the theoretical expectation. For the determination of m_t a kinematic fitting method is used. The most accurate mass determination is obtained for the lepton+jets channel. The present preliminary average [61, 62, 63] of all channels used is based on an integrated luminosity of 110 pb^{-1} and 115 pb^{-1} for the CDF and the DØ experiment, respectively:

$$m_t = 175 \pm 6 \text{ GeV}.$$

6. Global experimental picture of the Standard Model

In this section we would like to combine the data material discussed in the previous sections and show our present constraints on the Standard Model. The relevant input data are summarized in Table 6.

As explained in sections 1.4 and 2.1.3 the Standard Model allows us to predict all measurements, X_{meas}, with a few parameters:

$$X_{meas} = f(\alpha(m_Z^2),\, G_F,\, m_Z,\, m_t,\, m_H,\, \alpha_s(m_Z^2))$$

Amongst these parameters m_Z and m_t are measured directly at colliders, G_F is known precisely from muon decay [69]. Though the value of the fine structure constant at $s = m_e^2$ is most accurately measured, the value of $\alpha(m_Z^2)$ has a non-negligible error which arises from the contribution of light quarks to the photon vacuum polarization and is significant for the interpretation of these measurements (the uncertainty of $\alpha(m_Z^2)$ introduces e.g. an error of 0.00023 on the Standard Model prediction of $\sin^2\theta_{\text{eff}}^{\text{lept}}$). The result for $\alpha(m_Z^2)$ is obtained by applying a dispersion relation to the data available for the process $e^+e^- \to$ hadrons at different centre-of-mass energies. There have been several recent reevaluations [70, 71, 68, 72]. As stated in section 4. the strong coupling constant has been precisely measured in many processes. It is not included as input to any fit discussed below, as the data in Table 6 allow a precise determination of this parameter by themselves. So at present the only truly unknown parameter is m_H. The contribution of m_H in radiative corrections to precision observables is small and highly correlated with contributions of the top quark. Therefore, before the direct determination of m_t at the Tevatron, electroweak precision measurements were used to determine the mass of the top quark with m_H fixed arbitrarily to 300 GeV. The variation of results when varying

	Measurement with Total Error	Systematic Error	Standard Model	Pull
Z^0 boson mass and				
Z^0 fermion couplings at LEP 1				
line-shape and				
lepton asymmetries:				
m_Z [GeV]	91.1863 ± 0.0020	$^{(a)}0.0015$	91.1861	0.1
Γ_Z [GeV]	2.4946 ± 0.0027	$^{(a)}0.0017$	2.4960	−0.5
σ_h^0 [nb]	41.508 ± 0.056	0.055	41.465	0.8
R_ℓ	20.778 ± 0.029	0.024	20.757	0.7
$A_{FB}^{0,\ell}$	0.0174 ± 0.0010	0.007	0.0159	1.4
+ correlation matrix				
τ polarization:				
$\mathcal{A}_\tau$	0.1401 ± 0.0067	0.0045	0.1458	−0.9
$\mathcal{A}_e$	0.1382 ± 0.0076	0.0021	0.1458	−1.0
b and c quark results:				
$R_b{}^{(b)}$	0.2179 ± 0.0012	0.0009	0.2158	1.8
$R_c{}^{(b)}$	0.1715 ± 0.0056	0.0042	0.1723	−0.1
$A_{FB}^{0,b(b)}$	0.0979 ± 0.0023	0.0010	0.1022	−1.8
$A_{FB}^{0,c(b)}$	0.0733 ± 0.0049	0.0026	0.0730	0.1
+ correlation matrix Table				
$q\bar{q}$ charge asymmetry:				
$\sin^2\theta_{eff}^{lept}$ ($\langle Q_{FB}\rangle$)	0.2320 ± 0.0010	0.0008	0.23167	0.3
Z^0-fermion couplings at SLD				
$\sin^2\theta_{eff}^{lept}$ (A_{LR}[28])	0.23061 ± 0.00047	0.00014	0.23167	−2.2
R_b[41]$^{(b)}$	0.2149 ± 0.0038	0.0021	0.2158	−0.2
$\mathcal{A}_b$[64]	0.863 ± 0.049	0.032	0.935	−1.4
$\mathcal{A}_c$[64]	0.625 ± 0.084	0.041	0.667	−0.5
W-boson mass				
m_W [GeV] ($p\bar{p}$[45])	80.356 ± 0.125	0.110	80.353	0.0
$1 - m_W^2/m_Z^2$ (νN[65, 66, 67])	0.2244 ± 0.0042	0.0036	0.2235	0.2
direct measurement of m_t				
m_t [GeV] ($p\bar{p}$[61, 62, 63])	175 ± 6	4.5	172	0.5
electromagnetic coupling constant				
$\alpha(m_Z^2)^{-1}$[68]	128.896 ± 0.090	0.083	128.907	−0.1

Table 6: Summary of measurements included in the combined analysis of Standard Model parameters [25]. The total errors in column 2 include the systematic errors listed in column 3. The determination of the systematic part of each error is approximate. The Standard Model results in column 4 and the pulls (difference between measurement and fit in units of the total measurement error) in column 5 are derived from the Standard Model fit including all data (Table 7) with the Higgs mass treated as a free parameter.

$m_{\rm H}$ over the interval $60 \leq m_{\rm H}$ [GeV] ≤ 1000 was given as second error. The lower bound in this interval approximately corresponds to the limits obtained in direct searches, if the Higgs would be heavier than 1 TeV, electroweak interactions at high energies could no longer be treated perturbatively (of course, this is not an argument against $m_{\rm H}$>1 TeV, but then we could not trust our calculations any more).

Applying such a fit to all measurements except the direct $m_{\rm t}$ determination in Table 6 one obtains:

$$\begin{aligned} m_{\rm t} &= 177 \pm 7\,^{+16}_{-19}\ {\rm GeV} \\ \alpha_s(m_{\rm Z}^2) &= 0.121 \pm 0.003\ \pm 0.002 \end{aligned}$$

at a χ^2/d.o.f. of 20/14. If we were to find the Higgs, electroweak precision tests constrain $m_{\rm t}$ to $\pm$7 GeV, a precision comparable to the direct measurement. Until then the ignorance of $m_{\rm H}$ weakens this very strong test of our understanding of the quantum structure of the Standard Model by an additional uncertainty in $m_{\rm t}$ of approximately $\pm$20 GeV.

As the indirect and the direct determination of $m_{\rm t}$ are compatible they can also be combined. The result of a global fit is given in Table 7. Now the value of $m_{\rm t}$ is determined essentially by the direct measurement and the precision of the indirect measurements serves to determine $m_{\rm H}$. The error for $m_{\rm H}$ is still large and is asymmetric because radiative corrections are proportional to $\log m_{\rm H}$. Fig. 20 shows the value of $\Delta\chi^2 \equiv \chi^2 - \chi^2_{min}$ as a function of $\log m_{\rm H}$. The curve is obtained by varying $m_{\rm H}$ and minimizing all other parameters simultaneously. Also shown as a shaded band is the impact of theoretical errors due to missing higher orders. From this curve you can easily read off confidence intervals (c.f. e.g. [73, 74]). The upper bound on $m_{\rm H}$ at 95% confidence level (corresponding to $\Delta\chi^2 = 2.7$) amounts to $m_{\rm H} \leq 550$ GeV.

From the electroweak precision measurements we also obtain a value of $\alpha_s(m_{\rm Z}^2)$ which is in good agreement with other QCD studies but complementary in all aspects of theoretical and experimental uncertainties and of comparable precision as the world average.

The lower part of Table 7 lists results which can be derived from the fitted parameters. The value of $\sin^2\theta^{\rm lept}_{\rm eff}$ can also be obtained in a slightly less model dependent way, considering asymmetry measurements only: $\sin^2\theta^{\rm lept}_{\rm eff} = 0.23165 \pm 0.00024$.

$m_{\rm t}$ [GeV]	172 ± 6
$m_{\rm H}$ [GeV]	149^{+148}_{-82}
$\log(m_{\rm H})$	$2.17^{+0.30}_{-0.35}$
$\alpha_s(m_{\rm Z}^2)$	0.120 ± 0.003
χ^2/d.o.f.	19/14
$\sin^2\theta^{\rm lept}_{\rm eff}$	0.23167 ± 0.00023
$1 - m_{\rm W}^2/m_{\rm Z}^2$	0.2235 ± 0.0006
$m_{\rm W}$ (GeV)	80.352 ± 0.033

Table 7: Results of a fit to all data in Table 6 As the sensitivity to $m_{\rm H}$ is logarithmic, both $m_{\rm H}$ as well as $\log(m_{\rm H})$ are quoted. The bottom part of the table lists derived results for $\sin^2\theta^{\rm lept}_{\rm eff}$, $1 - m_{\rm W}^2/m_{\rm Z}^2$ and $m_{\rm W}$.

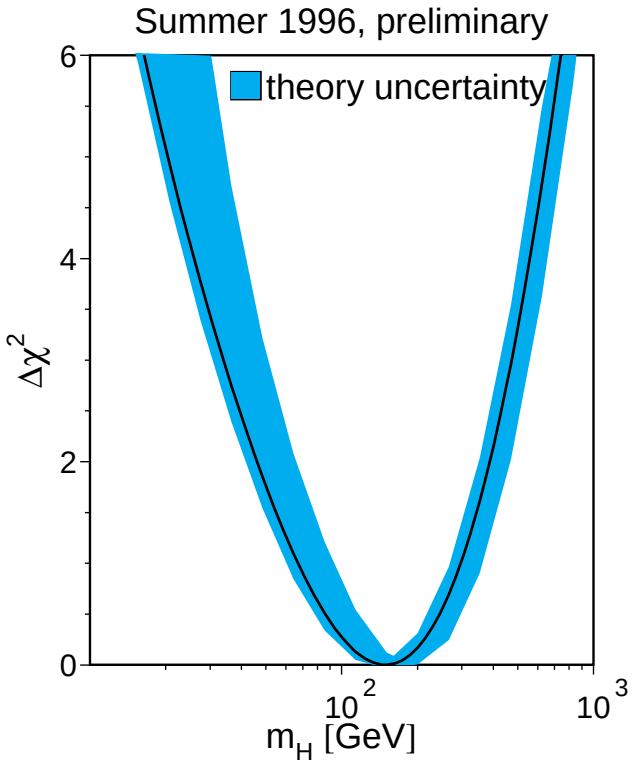

Figure 20: $\Delta\chi^2 = \chi^2 - \chi^2_{min}$ vs. $m_{\rm H}$ curve. The line is the result of the fit using all data (Table 7); the band represents an estimate of the theoretical error due to missing higher order corrections.

7. Summary and outlook

Colliders provide excellent facilities to pin down the Standard Model as a very solid null hypothesis.

Strange enough, we have no experimental hint why the Standard Model works so well: Stringent tests of radiative corrections make it appear to us as if it were a gauge theory. For the moment only your text books tell you how a gauge theory can be compatible with the observation of massive gauge bosons and fermions. And if the mechanism described there is true you should soon witness the discovery of a Higgs boson.

Also, as discussed in other lectures at this school, the Standard Model has many open questions and we are convinced today, that it will break down at high energies. But up to now we have no experimental hint for a theory embedding the Standard Model.

It will be up to you to explore these questions and colliders will be an important tool with a promising near-future program:

- Final LEP 1 and Tevatron analyses of run I with many interesting results which will also contribute significantly to our understanding of the heavy quark sector (c, b, t).
- More statistics from SLC and HERA.
- After the successful start of LEP 2 there is hope for an integrated luminosity of 500 pb^{-1} which will definitively give us a detailed understanding of the physics with W-bosons but there are also good chances for discoveries (Higgs ?, SUSY ?, ...).
- In 1999 after the upgrade, Tevatron will restart with significantly increased luminosity and improved detectors.

– In 2005 we expect first collisions of 7 TeV protons on 7 TeV protons at LHC.
– New interesting collider projects are under discussion. Especially for a linear e^+e^- collider there exist already detailed studies of its physics potential and its technical feasibility accompanied by R&D work at several laboratories.

Acknowledgements
It is a pleasure to thank the organizers for their invitation to this school. I very much enjoyed the stimulating atmosphere with lots of exciting events and I would like to congratulate the organizers for their exceptional talent to make this school a great success.

REFERENCES

[1] ALEPH Collaboration, D. Decamp et al., Nucl. Instr. and Meth. **A294** (1990) 121.
[2] DELPHI Collaboration, P. Aarnio et al., Nucl. Instr. and Meth. **A303** (1991) 233.
[3] L3 Collaboration, B.Adeva et al., Nucl. Instr. and Meth. **A289** (1990) 35.
[4] OPAL Collaboration, K. Ahmet et al., Nucl. Instr. and Meth. **A305** (1991) 275.
[5] LEP Energy Working Group, R. Assmann et al., Z. Phys. **C66** (1995) 567.
[6] Mark II Collaboration, G.S. Abrams et al., Nucl. Instr. and Meth. **A281** (1989) 55.
[7] SLD Collaboration, *The SLD Design Report*, SLAC Report 273, 1984.
[8] CDF Collaboration, F. Abe et al., Nucl. Instr. Meth. **A271** (1988) 387.
[9] DØ Collaboration, S. Abachi et al., Nucl. Instr. Meth. **A338** (1994) 185.
[10] H1 Collaboration, *The H1 detector at HERA*, DESY 96-01, March 1996.
[11] ZEUS Collaboration, *The ZEUS Detector: Status Report 1993*, ZEUS-STATUS-REPT-1993, Feb 1993.
[12] UA1 Collaboration, G. Arnison et al., Phys. Lett. **122B** (1983) 103;
UA2 Collaboration, M. Banner et al., Phys. Lett. **122B** (1983) 476;
UA1 Collaboration, G. Arnison et al., Phys. Lett. **126B** (1983) 103;
UA2 Collaboration, P. Bagnaia et al., Phys.Lett. **129B** (1983) 130.
[13] TASSO Collaboration, R. Brandelik et al., Phys. Lett. **86B** (1979) 243;
for a review of physics at PETRA s. S.L. Wu, Phys. Rep. **107** (1984) 59.
[14] ALEPH Collaboration, D. Decamp et al., Z. Phys. **C48** (1990) 365;
ALEPH Collaboration, D. Decamp et al., Z. Phys. **C53** (1992) 1;
ALEPH Collaboration, D. Buskulic et al., Z. Phys. **C60** (1993) 71;
ALEPH Collaboration, D. Buskulic et al., Z. Phys. **C62** (1994) 539;
ALEPH Collaboration, *Preliminary Results on Z Production Cross Section and Lepton Forward-Backward Asymmetries using the 1990-1995 Data*, contributed paper to ICHEP96, Warsaw, 25-31 July 1996, **PA-07-069**.
[15] DELPHI Collaboration, P. Aarnio et al., Nucl. Phys. **B367** (1991) 511;
DELPHI Collaboration, P. Abreu et al., Nucl. Phys. **B417** (1994) 3;
DELPHI Collaboration, P. Abreu et al., Nucl. Phys. **B418** (1994) 403;
DELPHI Collaboration, DELPHI Note 95-62 PHYS 497, July 1995;
DELPHI Collaboration, DELPHI Note 96-118 CONF 65, contributed paper to ICHEP96, Warsaw, 25-31 July 1996, **PA-07-001**.

[16] L3 Collaboration, B. Adeva et al., Z. Phys. **C51** (1991) 179;
L3 Collaboration, O. Adriani et al., Phys. Rep. **236** (1993) 1;
L3 Collaboration, M. Acciarri et al., Z. Phys. **C62** (1994) 551;
L3 Collaboration, *Preliminary L3 Results on Electroweak Parameters using 1990-95 Data*, L3 Note 1980, August 1996.

[17] OPAL Collaboration, G. Alexander et al., Z. Phys. **C52** (1991) 175;
OPAL Collaboration, P.D. Acton et al., Z. Phys. **C58** (1993) 219;
OPAL Collaboration, R. Akers et al., Z. Phys. **C61** (1994) 19;
OPAL Collaboration, *A Preliminary Update of the* Z^0 *Line Shape and Lepton Asymmetry Measurements with the 1993 and 1994 Data*, OPAL Physics Note PN166, Febuary 1995;
OPAL Collaboration, *The Preliminary OPAL SiW luminosity analysis: Results for the 1994 Summer conferences*, OPAL Physics Note PN142, July 1994;
OPAL Collaboration, *A Preliminary Update of the Z Line Shape and Lepton Asymmetry Measurements with a Revised 1993-1994 LEP Energy and 1995 Lepton Asymmetry*, OPAL Physics Note PN242, July 1996;
OPAL Collaboration, *Measurements of Lepton Pair Asymmetries using the 1995 Data*, contributed paper to ICHEP96, Warsaw, 25-31 July 1996 **PA07-015**.

[18] A. Arbuzov, et al., Phys. Lett. **B383** (1996) 238;
S. Jadach, et al., "Upgrade of the Monte Carlo program BHLUMI for Bhabha scattering at low angles to version 4.04", CERN-TH/96-156, UTHEP-96-0601, June 1996, submitted to Comp. Phys. Comm..

[19] A. Sokolov and I.M. Ternov, Sov. Phys. Doklady **8** (1964) 1203.

[20] M. Caffo et al., *Bhabha Scattering*, in [75], Vol. 1, p. 171.

[21] W. Hollik, *Electroweak Theory*, KA-TP-4-1996, Sep 1995. Lectures at the 5th Hellenic School and Workshops on Elementary Particle Physics, 3-24 Sep 1995, Corfu, Greece.

[22] *Reports of the working group on precision calculations for the Z resonance*, eds. D. Bardin, W. Hollik and G. Passarino, CERN Yellow Report 95-03, Geneva, 31 March 1995.

[23] M. Consoli, W. Hollik and F. Jegerlehner *Electroweak radiative corrections for Z Physics*, in [75], Vol. 1, p. 7.

[24] The LEP Collaborations ALEPH, DELPHI, L3, OPAL and the LEP Electroweak Working Group, *Updated Parameters of the* Z^0 *Resonance from Combined Preliminary Data of the LEP Experiments*, CERN-PPE/93-157.

[25] The LEP Collaborations ALEPH, DELPHI, L3, OPAL and the LEP Electroweak Working Group, *A Combination of Preliminary Electroweak Measurements and Constraints on the Standard Model*, CERN-PPE/96-183.

[26] C.Y. Prescot et al., Phys. Lett. **B77** (1978) 347 and **B84** (1979) 524.

[27] M.A. Bouchiat and L. Pottier, Science **234** (1986) 1203;
M.C. Noecker et al., Phys. Rev. Lett. **61** (1988) 310;
S.A. Blundell, W.R. Johnson and J. Saphirstein, Phys. Rev. Lett. **65** (1990) 1411.

[28] SLD Collaboration, E. Torrence, *Determination of Electroweak Parameters at the SLC*, talk presented at ICHEP96, Warsaw, 25-31 July 1996;
K. Abe et al., Phys. Rev. Lett. **73** (1994) 25;
K. Abe et al., Phys. Rev. Lett. **70** (1993) 2515.

[29] D. Bardin et al., Z. Phys. **C44** (1989) 493; Comp. Phys. Comm. **59** (1990) 303; Nucl. Phys. **B351**(1991) 1; Phys. Lett. **B255** (1991) 290 and CERN-TH 6443/92 (May 1992).

[30] SLD Collaboration, Z^0 *pole measurements of parity violation parameters* $\mathcal{A}_b$ *and* $\mathcal{A}_c$ *at SLC / SLD*, D. Falciai, talk presented at ICHEP96, Warsaw, 25-31 July 1996, SLAC-PUB-7334.

[31] The LEP Experiments : ALEPH, DELPHI, L3, OPAL; Nucl. Instr. Meth. **A378** (1996) 101.

[32] ALEPH Collaboration, D. Buskulic et al., Z. Phys. **C62** (1994) 179;
ALEPH Collaboration, D. Buskulic et al., Phys. Lett. **B384** (1996)414;
ALEPH Collaboration., D. Buskulic et al., *Measurement of the semileptonic b branching ratios from inclusive leptons in Z decays*, Contributed Paper to EPS-HEP-95 Brussels, **eps0404**.

[33] DELPHI Collaboration, P.Abreu et al., Z. Phys. **C66** (1995) 323.

[34] L3 Collaboration, O. Adriani et al., Phys. Lett. **B292** (1992) 454;
L3 Collaboration, M. Acciarri et al., Phys. Lett. **B335** (1994) 542;
L3 Collaboration, *Measurement of* R_b *and BR(*$b \to \ell X$*) from b-quark semileptonic decays,* L3 Note 1449, July 16 1993;
L3 Collaboration, *L3 Results on* $A_{FB}^{b\bar{b}}$, $A_{FB}^{c\bar{c}}$ *and* χ *for the Glasgow Conference,* L3 Note 1624;
L3 Collaboration, *L3 Results on* R_b *and* $BR(b \to \ell)$ *for the Glasgow Conference,* L3 Note 1625.

[35] OPAL Collaboration, G. Alexander et al., Z. Phys. **C70** (1996) 357;
OPAL Collaboration, R. Akers et al., *Updated Measurement of the Heavy Quark Forward-Backward Asymmetries and Average B Mixing Using Leptons in Multihadronic Events*, OPAL Physics Note PN226 contributed paper to ICHEP96, Warsaw, 25-31 July 1996 **PA05-007**.

[36] L3 Collaboration, O. Adriani et al., Phys. Lett. **B307** (1993) 237.

[37] ALEPH Collaboration, *Measurement of* R_b *using a Lifetime-Mass Tag*, contributed paper to ICHEP96, Warsaw, 25-31 July 1996 **PA10-014**;
ALEPH Collaboration, *A Measurement of* R_b *using Mutually Exclusive Tags*, contributed paper to ICHEP96, Warsaw, 25-31 July 1996 **PA10-015**.

[38] DELPHI Collaboration, P.Abreu et al., Z. Phys. **C70** (1996) 531;
DELPHI Collaboration, P. Abreu et al., *Measurement of the partial decay width* $R_b = \Gamma_{b\bar{b}}/\Gamma_{had}$ *with the DELPHI detector at LEP* , contributed paper to ICHEP96, Warsaw, 25-31 July 1996 **PA01-061**.

[39] L3 Collaboration, *Measurement of the Z Branching Fraction into Bottom Quarks Using Lifetime Tags*, contributed paper to ICHEP96, Warsaw, 25-31 July 1996 **PA05-049**.

[40] OPAL Collaboration, R. Akers et al., Z. Phys. **C65** (1995) 17;
OPAL Collaboration, *An Update of the Measurement of* $\Gamma_{b\bar{b}}/\Gamma_{had}$ *using a Double Tagging Method*, OPAL Physics Note PN181, contributed paper to EPS-HEP-95 Brussels, **eps0278**.

[41] SLD Collaboration, G. Crawford, talk presented at ICHEP96, Warsaw, 25-31 July 1996.

[42] ALEPH Collaboration, *Measurement of the partial decay width of the Z into $c\bar{c}$ quarks* contributed paper to ICHEP96, Warsaw, 25-31 July 1996 **PA10-016**.

[43] DELPHI Collaboration, *Summary of R_c measurements in DELPHI,* DELPHI 96-110 CONF 37 contributed paper to ICHEP96, Warsaw, 25-31 July 1996 **PA01-060**.

[44] OPAL Collaboration, R. Akers et al., Z. Phys. **C67** (1995) 27;
OPAL Collaboration, G. Alexander et al., Z. Phys. **C72** (1996) 1;
OPAL Collaboration, *A measurement of $BR(\mathrm{c} \to \mathrm{D}^\star)$ and $\Gamma_{c\bar{c}}/\Gamma_{had}$ using a double tagging method*, OPAL Physics Note PN227 contributed paper to ICHEP96, Warsaw, 25-31 July 1996 **PA05-011**.

[45] M. Rijssenbeek, talk presented at ICHEP96, Warsaw, 25-31 July 1996.

[46] M. Demarteau, Precision Electroweak Measurements, Proceedings DPF'96, Minneapolis, August 10-15, 1996, FERMILAB-CONF-96/354.

[47] Z. Kunszt et al., *Determination of the mass of the W boson*, in [76], Vol. 1, p. 141.

[48] R. Clare, Aspen Winter Conference on Particle Physics, January 19-25, 1997.

[49] L.J. Nodulman, *Diboson production at the Tevatron*, Proceedings ICHEP96, Warsaw, 25-31 July 1996, FERMILAB-Conf-96/326-E.

[50] G. Gounaris et al., *Triple gauge boson couplings*, in [76], Vol. 1, p. 525.

[51] S. Bethke and J. Pilcher, Annu. Rev. Nucl. Part. Sci. **42** 1992 251.
S. Bethke, *Hadronic physics in electron-positron annihilation*, 42nd Scottish Universities Summer School in Physics, St. Andrews, UK, 1 - 21 Aug 1993, Proceedings K J Peach, L L J Vick and P Osborne, SUSSP, Bristol, 1994 79-127.
Th. Hebbeker, Phys. Rep. **217C** (1992) 69.

[52] Michael Schmelling, *Status of the strong coupling constant*, Proceedings ICHEP96, Warsaw, 25-31 July 1996.

[53] ZEUS Collaboration, M. Derrick et al., Phys. Lett **363B** (1995) 201.

[54] H1 Collaboration, T. Ahmed et al., Phys. Lett **B346** (1995) 415.

[55] S. Bethke, *Experimental tests of asymptotic freedom*, Proceedings of the QCD Euroconference 96, Montpellier, July 4-12, 1996.

[56] S. W. Herb et al., Phys. Rev. Lett. **39** (1977) 252-255.

[57] UA1 Collaboration, G. Arnison et al. Phys. Lett. **147B** 493.

[58] CDF Collaboration, F. Abe et al., Phys. Rev. Lett. **73** (1994) 225.

[59] CDF Collaboration, F. Abe et al., Phys. Rev. Lett. **74** (1995) 2626.

[60] DØ Collaboration, S. Abachi et al., Phys. Rev. Lett. **74** (1995) 2632.

[61] CDF Collaboration, J. Lys, talk presented at ICHEP96, Warsaw, 25-31 July 1996.

[62] DØ Collaboration, S. Protopopescu, talk presented at ICHEP96, Warsaw, 25-31 July 1996.

[63] P. Tipton, talk presented at ICHEP96, Warsaw, 25-31 July 1996.

[64] SLD Collaboration, D. Falciai, talk presented at ICHEP96, Warsaw, 25-31 July 1996.

[65] CDHS Collaboration, H. Abramowicz et al., Phys. Rev. Lett. **57** (1986) 298;
CDHS Collaboration, A. Blondel et al., Z. Phys. **C45** (1990) 361.

[66] CHARM Collaboration, J.V. Allaby et al., Phys. Lett. **B177** (1986) 446;
CHARM Collaboration, J.V. Allaby et al., Z. Phys. **C36** (1987) 611.

[67] CCFR Collaboration, K. McFarland, *An improved measurement of $\sin^2\theta_W$ from neutrino-nucleon deep inelastic scattering*, proceedings of the XV workshop on Weak

Interactions and Neutrinos, Talloires France, G. Bonneaud *et al.* eds., Tufts University and L.A.L. Orsay (Sept.1996) vol. II p. 607.
[68] S. Eidelmann and F. Jegerlehner, Z. Phys. **C67** (1995) 585.
[69] R.M. Barnett et al., Phys. Rev. **D54** (1996) 1.
[70] M. L. Swartz, Phys. Rev. **D53** (1996) 5268.
[71] A.D. Martin and D. Zeppenfeld, Phys. Lett. **B345** (1994) 558.
[72] H. Burkhardt and B. Pietrzyk, Phys. Lett. **B356** (1995) 398.
[73] W.T. Eadie et al., *Statistical Methods in Experimental Physics*, North-Holland Publishing Company, 1971.
[74] Frodesen et al., *Probability and Statistics in Particle Physics*, Universitetsforlaget, Bergen, 1979.
[75] Proceedings of the Workshop on *Z Physics at LEP1*, CERN 89-08, Sept. 1989, ed. G. Altarelli, R. Kleiss and C. Verzegnassi.
[76] *Physics at LEP 2*, ed. G. Altarelli, T. Sjostrand and F. Zwirner, CERN 96-01.